NASA TMX-55199

X-650-65-64

INVESTIGATION OF THE MAJOR CONSTITUENTS OF THE APRIL-MAY 1963 HETEROSPHERE BY THE EXPLORER XVII SATELLITE

BY

CARL A. REBER

MARCEL NICOLET

[redacted]

FEBRUARY 1965

NASA — GODDARD SPACE FLIGHT CENTER

GREENBELT, MARYLAND

INVESTIGATION OF THE MAJOR CONSTITUENTS OF THE APRIL-MAY 1963 HETEROSPHERE BY THE EXPLORER XVII SATELLITE

by

Carl A. Reber
Goddard Space Flight Center
Greenbelt, Maryland

and

Marcel Nicolet
National Center for Space Research
3 Avenue Circulaire
Brussels, Belgium

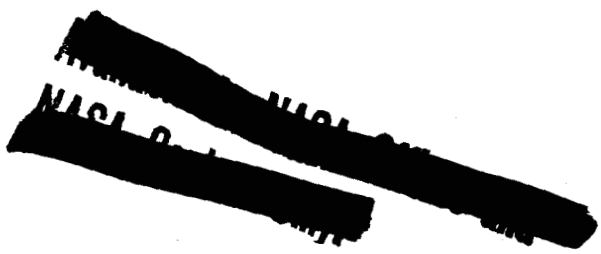

ABSTRACT

18327

The mass spectrometer experiment on the Explorer XVII satellite has yielded new data on the concentrations of the major components of the neutral upper atmosphere over a two month period in the spring of 1963. These data compare favorably with results from the total density experiments on the same spacecraft as well as satellite drag data and direct measurements made from rockets. The night measurements are in general consistent with an isothermal atmosphere at a temperature of 650° to 700°K while the daytime scale heights indicate a temperature of 825° ± 75°K. There was a large variability in the number densities at a given altitude, indicating a strong sensitivity to changes in energy inputs to the atmosphere, particularly to changes in magnetic activity. Average quiet daytime conditions near 260 kilometers altitude were observed to be: N_2, $1.5 \pm 0.5 \times 10^8$ cm^{-3}; 0, $2.4 \pm 0.4 \times 10^8$ cm^{-3}; He, $1.4 \pm 0.3 \times 10^6$ cm^{-3}. Average quiet nighttime conditions at 400 kilometers were: N_2, $2.0 \pm 1.0 \times 10^6$ cm^{-3}; 0, $1.0 \pm 0.4 \times 10^7$ cm^{-3}; He, $6.0 \pm 2.0 \times 10^5$ cm^{-3}. The large horizontal change in the location of the satellite during a measurement precludes the interpretation of the data in terms of a simple vertical profile, but does offer the possibility of investigating local time or other horizontal gradient effects on the atmospheric constituents.

1. INTRODUCTION

Prior to 1963 aeronomic measurements in the upper atmosphere fell into two categories; a rather small number of direct measurements by means of sounding rockets and indirect measurements based on deductions from satellite drag accelerations. The rocket experiments yielded results in terms of density, pressure and composition in the altitude range 100-220 kilometers and generally over specific locations on the earth's surface, such as White Sands, N. M., Fort Churchill, Canada, or Wallops Island, Virginia (J. W. Townsend, et al, 1954)[1], (J. W. Townsend and E. B. Meadows, 1958)[2,3], (A. O. Nier, et al, 1964)[4], (A. A. Pokhunkov, 1963)[5], (E. Meadows-Reed and C. R. Smith, 1964)[6], (E. J. Schaefer and M. H. Nichols, 1963)[7], (D. R. Taeusch, et al)[8], (L. M. Jones, 1954)[9]. From satellite drag data on the other hand it is possible to obtain continuous monitoring at various altitudes corresponding to the perigee altitudes of particular satellites and generally above 200 kilometers (G. V. Groves, 1961)[10], (R. Jastrow and R. Bryant, 1960)[11], (L. G. Jacchia, 1963)[12], (H. K. Paetzold, 1959)[13], (D. G. King-Hele and D.M.C. Walker, 1961)[14], However, the information gathered from drag accelerations is in the form of $\rho H^{1/2}$, where ρ is the total density and H is the atmospheric scale height, and this quantity has proven to be ambiguous as evidenced by the number of apparently conflicting atmospheric models based on the same observations. Drag data have, nonetheless, provided the bulk of the atmospheric information at altitudes greater than 200 kilometers. They have demonstrated the extreme variability of the upper atmosphere and indicated the major

cause for these variations to be excursions in the solar flux incident on the atmosphere.

The Explorer XVII aeronomy satellite was launched on 2 April 1963, with the purpose of extending the techniques previously used in rocket measurements to higher altitudes and to provide a much broader coverage than had been achieved. It carried four pressure gages (G. P. Newton, et al, 1965)[15], two mass spectrometers and two electrostatic probes to measure electron energies and ion density (L. H. Brace, et al, 1965)[16]. The purpose of this paper is to present the majority of the data from the mass spectrometer experiment as well as preliminary interpretations of the atmospheric phenomena observed. Good data were received from one of the spectrometers for approximately 187 real time interrogations (passes) covering a two month time span following launch. Data from the other spectrometer indicate a malfunction in the system and will not be reported here.

2. EXPERIMENT

2.1 General

Previous measurements of composition in the upper atmosphere as well as a number of theoretical investigations (M. Nicolet, 1961)[17, 18] had indicated that the major constituents in the altitude range covered by Explorer XVII would be molecular nitrogen, atomic oxygen, and possibly, helium. Therefore, these three gases were the primary ones investigated with the mass spectrometers, although molecular oxygen, atomic nitrogen and water vapor (which might have affected the atomic oxygen measurement) were also monitored.

The spin stabilized Explorer XVII (N. W. Spencer, 1965)[19] was injected into an orbit of 58° inclination, 257 kilometer perigee and 900 kilometer apogee, with a spin rate of 90 revolutions per minute. Perigee was initially at 40° north latitude and moved north to 58° and then south to 20° south latitude during the operating lifetime of the satellite. As there was no data storage facility on board Explorer XVII, these orbit parameters are particularly important as they determine the relationship between local sun time and altitude for passes of the satellite over any one ground receiving station. It is the summation of data from all the ground stations which allows diurnal/altitude variations to be observed, even though this injects a geographic variation as well.

Physically, the satellite was a stainless steel sphere, 35 inches in diameter, constructed using state-of-the-art techniques in vacuum system design. The two mass spectrometers were located on the opposite ends of the spin axis, which at launch was nearly in the plane of the orbit. Primary power was supplied by wet cell batteries from which was obtained a lifetime of greater than three months. Data were transmitted via a 9 bit pulse code modulation telemetry system, offering a precision in reading the data of approximately 0.2%.

Usable data were not obtained from the mass spectrometer over the full satellite lifetime for two reasons. At the end of 290 orbits the spin axis had precessed in such a way as to point the spectrometer directly at the sun. As there was then no chance to dissipate all the incident energy, the spectrometer and attached detector amplifier reached quite

high temperatures (94°C on the spectrometer mount). At these temperatures the output of the amplifier was degenerated. By orbit 700 the spin axis had precessed sufficiently for the spectrometer and amplifier to cool to operating temperatures.

By orbit 900 the amplifier output again appeared to be degenerating. This degeneration took the form of a large drift in zero level and an apparent decrease in voltage gain for the system. One possible explanation for this is the cumulative effect of energetic particles on the high impedance portions of the electrometer circuit. The amplifier did not recover from this degeneration.

2.2 The Mass Spectrometer

The velocity of the satellite, about eight kilometers a second, was high compared to the mean thermal velocity of the ambient gas particles. This caused the neutral particles to approach with a kinetic energy which varied directly with their mass and which ranged between 12 electron volts for molecular oxygen down to 0.67 ev for helium. Since the particles approached anti-parallel to the satellite velocity vector there was, in effect, a flux of particles beamed at the spectrometer. The angle of incidence of this beam was dependent on the orientation of the satellite with respect to its velocity vector. The requirement to analyze particles incident in this manner dictated, to a large extent, the overall design of the experiment (E. B. Meadows, 1960)[20], (L. G. Hall, et al, 1960)[21], (N. W. Spencer and C. A. Reber, 1963)[22], (C. A. Reber and L. G. Hall, 1965)[23].

The mass spectrometer employed was a double focusing magnetic deflection type designed specifically for satellite use (Figure 1). Its design featured a "nude" electron beam ion source external to the satellite surface and an ion lens to focus the energetic ions formed from the high velocity incident neutral particles. The electric and magnetic fields of the analyzer were held constant and mass selection was achieved by stepping between preselected ion collectors located along the spectrometer focal plane.

The ion current incident on the collectors was detected by a sensitive electrometer amplifier. The output of the electrometer was fed into a logarithmic amplifier which compressed its large dynamic range into a form suitable for telemetry. With the precision which the telemetry allowed, the output of the electrometer reading, through the log amp, was known to within 1.5 to 2.0%.

Figure 2 is a photograph of a telemetry record showing the output of the logarithmic amplifier. Each data step is four seconds in length and there are two sensitivity ranges (differing by a factor of 100) incorporated into the linear electrometer amplifier. The calibration sequence in the middle of the run is from an in-flight calibrator for the detector system.

The "rezero sample" step in each cycle is the result of the operation of a circuit in the electrometer amplifier designed to minimize the influence of dc drift of the zero level by once each cycle clamping the zero level to ground potential. Following the zero level monitor the

masses are sampled in the sequence He (4), N (14), H_2O (18), O_2 (32), N_2 (28), O (16) and total. This particular sequence was chosen to sample the constituents in order of their expected abundances, with the highest currents measured last. Thus the effect of any small drift in the zero level, following the rezero operation, would be minimized. This drift was measured in test to be about one millivolt per minute.

2.3 Experiment Calibration

The mass spectrometer was calibrated on a high vacuum system using two or more commercial (Veeco, Westinghouse, and Varian) Bayard-Alpert pressure gages. These gages were calibrated against other Bayard-Alpert type pressure gages which in turn had been calibrated against a McCleod absolute pressure gage. This family of calibrated gages includes those against which the pressure gages on Explorer XVII (G. P. Newton, et al, 1965)[15] and the omegatron partial pressure gages flown in the Thermosphere Probes (N. W. Spencer, et al, 1965)[24] were calibrated.

The system was pumped to its ultimate vacuum, in the low 10^{-9} torr range, and a background spectrum was obtained. A pure sample gas N_2, O_2 or He was then admitted in small increments and the readings of the pressure gages and the spectrometer recorded. This was continued to a maximum pressure of 10^{-5} torr for He and N_2, or to 10^{-7} for O_2, and then the sample gas pressure was decreased in small increments. After correction for the background contributions and chemical effects (e.g. formation of CO upon introduction of oxygen) a least squares analysis

was run on the data to obtain the calibration constant for each gas. Data from the increase and decrease of sample pressure were used in the analysis and were quite consistent. The sensitivity of the mass spectrometer for atomic oxygen was calculated using the results of the molecular oxygen calibration and the data of Fite and Brackman (W. L. Fite and R. T. Brackman, 1959)[25] on the ratio of cross sections of atomic and molecular oxygen as a function of the energy of the ionizing electrons.

This calibration was carried out at least three times on as many days before the entire mass spectrometer system was subjected to environmental testing in the form of launch vibration simulation. Following vibration the calibration procedure was repeated to test for any change in system performance. The six separate calibrations were repeatable within the limits of reading the laboratory pressure gage control units, or about 3%.

2.4 Data Analysis

The primary task of data analysis was to convert the telemetered ion currents into number densities of the ambient constituents. These ion currents were direct measurements of the number densities of the gases in the ion source, or sampling volume, at the time of the measurement. In general, particles could arrive in this sampling volume from the atmosphere in one of three ways: (1) ambient particles could enter the source volume directly, with no prior surface collisions, and become ionized; (2) particles could become ionized after having undergone one or more surface interactions in the source region and having become

partially thermalized; (3) particles could enter the spectrometer, become completely thermalized, and pass through the sampling volume upon being re-emitted from the spectrometer. (A thermalized particle is one which has undergone a sufficient number of surface collisions to reduce its high initial kinetic energy to approximately 0.025 ev, equivalent to the satellite temperature). By studying these three cases and combining the results with the laboratory gas calibrations, the relationship between the measured ion currents and the ambient concentrations could be deduced.

Despite the precautions taken to minimize the amount of gas background from the spectrometer there was still some contamination evident under certain measurement conditions. At times when the spectrometer opening was pointing "backward" along the satellite velocity vector there was no ram buildup of particles; on the contrary, the number of particles entering the gage from the atmosphere was negligible due to the large difference in velocities of the satellite and gas particles. (R. Horowitz and H. E. LaGow, 1957)[26]. Measurements at these times, however, indicated non-vanishing partial pressures for all the components with the exception of helium; these measurements indicated the gage background pressures, due to desorption, for the various gases. Over the course of the satellite lifetime there was a sufficient number of these background measurements to allow construction of an outgassing history for each gas; the background contribution at the time of each atmospheric measurement was then subtracted from the measurement.

The analysis procedure was then to (1) ascertain the background to subtract for a given measurement and (2) multiply the remainder by the appropriate function to relate the measurement to the atmosphere:

$$N_{ja} = \frac{N_{jm} - N_{jBKG}}{K_j(\alpha)},$$

where N_{ja} is the ambient number density of the j^{th} component N_{jm} is the measured number density, N_{jBKG} is the appropriate background density and $K_j(\alpha)$ is the factor relating the measurement to the atmosphere as a function of the angle between the gage normal and the satellite velocity vector (angle of attack, α). $K_j(\alpha)$ is shown in Figure 3.

The absolute accuracy of the number density data is ±40%, reflecting laboratory vacuum calibration error and the uncertainties in the ambient number density calculations. The relative accuracy for a given component varies with the difference in the angles of attack for the passes being compared. For passes where the angles of attack are similar the relative accuracy is about 3%; for data obtained where the angles of attack differ by 70° or more, the relative accuracy is about 20%. For different components the relative accuracy on the same pass is within 20%. This allows the mean mass to be assigned a worst case accuracy of 6%. This worst case is for a mixture which is essentially the two components helium and atomic oxygen in equal parts. For an atomic oxygen density ten times that of helium, the error drops to less than 0.6%. For equal parts molecular nitrogen and atomic oxygen the mean mass error is less than 3%; it also decreases as we increase one component or the other.

Since the relative accuracy of the number density varies with the angle of attack, this quantity is listed in Table I, along with the local suntime and other pertinent information.

3. DATA

The data were taken over geographic areas centered on the locations of the Minitrack ground receiving stations. The relationships between altitude and local time for the passes from which mass spectrometer data are presented are shown in Figure 4. This altitude-time relationship is determined by orbital parameters including the motion of the subperigee point. It can be seen from the figure that there is a strong interrelationship between any altitude profile and local time changes.

Ambient number densities as a function of altitude are shown in Figures 5, 6 and 7 and 10 through 14. These are the data arrived at by the procedures outlined in the preceding section. Figures 5, 6 and 7 show data from passes with local time between 4.00 hours and 21.00 hours, or roughly the daytime passes, while Figures 10 through 14 contain the nighttime data. Atomic oxygen and molecular nitrogen data obtained from a single satellite pass are indicated by a pair of points joined by a straight line.

Data from passes specifically referenced in the text or of particular interest are indicated on the figures by the orbit number and receiving station. These stations and the abbreviations used are as follows: Blossom Point, Md. (BP); College, Alaska (COL); Fort Myers, Fla. (FTM);

Grand Forks, Minn. (GFO); Quito, Equator (QUI); Mojave, Calif. (MOJ); Newfoundland (NFL); Woomera, Australia (OOM); Johannesburg, South Africa (JOB); Winkfield, England (WNK).

Due to the low signal to noise for the helium data we have had to reject two out of the three helium measurements per pass. This was due to a small, unknown zero offset in the electrometer amplifier output at the time of the first and third measurement. There is thus only one helium data point presented for each pass. All the measurements presented here from a single pass, N_2, O and He, were taken within one minute of each other in real time and each data point shown represents an average over two seconds in time and therefore an average of 120 telemetered data points. This two seconds represents 16 km or less in displacement of which no more than 0.75 km is vertical motion.

The total mass density, as obtained from the mass spectrometer, is shown as a function of altitude in Figures 8 and 15. This quantity was obtained by summing the contributions of the major constituents, atomic oxygen, molecular nitrogen and helium, for each pass according to the formula $\rho = \Sigma n_i m_i$; n_i is the number density of the i^{th} component and m_i is its mass. As the measurements for each gas are made at different real times, and hence at different altitudes, the number densities are extrapolated or interpolated within a pass to arrive at two reference altitudes per pass for the total density.

Figures 9 and 16 show the mean molecular mass, $M = \Sigma_i n_i M_i / \Sigma n_i$ (where M_i is the atomic mass number of the i^{th} species), as a function

of altitude. Here again the points shown are extrapolated or interpolated within a pass to arrive at two reference altitudes. In this case only the number densities of N_2, O and He are used, any other measured component having a negligible effect on the result. It should be pointed out that the omission of hydrogen, which the instrument was not designed to measure, could raise the calculated mean mass over the actual value at the higher altitudes.

4. DISCUSSION

4.1 Nighttime Molecular Nitrogen

By neglecting, for the time being, those nighttime data taken at times of known geomagnetic or solar disturbances one can obtain a general idea of the variation of the N_2, He and O concentrations in the altitude range from 300 km to 500 km. Passes 163 WNK, 167 BP and 182 BP (Figure 5) occurred on 14 and 15 April and apparently reflected the effect of a small magnetic disturbance, $A_p = 17$, on the 14th. The remainder of the passes shown in this altitude range exhibit an overall decrease in N_2 concentration with altitude which is consistent with a diffusion controlled atmosphere at a temperature of about 700°K and an absolute concentration at 400 km of $2.0 \pm 1.0 \times 10^6$ per cubic centimeter.

The variations within individual passes, which do not appear to follow the general altitude profile, can be understood in part on the basis of the local time variation between the two measurements. For the data shown in Figure 5 the lower altitude measurement is made in general about one half hour in local time before the higher altitude

measurement; e.g. pass 237 WNK measured N_2 at 22.56 hours and 23.16 hours. A difference of about 30° in the local temperature for the two measurements would account for the difference observed between the slope for this pass and the slope for an atmospheric temperature of 700°.

There is, of course, a local time variation from pass to pass in the data shown in Figure 5. This variation works in such a way as to place the lower altitude data, 300 to 375 km, generally earlier in the evening than the higher altitude data; for example, we see that 237 WNK occurred around 23.00 hours while 138 BP was monitored at 2.50 hours. There thus has been a longer time interval since sunset for the high altitude passes. This, combined with the tendency for equilibrium to occur first at higher altitudes due to the inverse dependence of diffusion time on number density, would act to decrease the relative concentrations of N_2 at higher altitudes with respect to that observed below 400 kilometers.

As mentioned earlier, passes 163 WNK, 167 BP and 182 BP were taken at the time of a small magnetic disturbance, $A_p = 17$, and show an increase of about a factor of three in N_2 concentrations over the measurements made at times of lower A_p. On the other hand, pass 119 WNK corresponds to a time when A_p was particularly low with a value of 2, and this pass indicated N_2 densities lower by more than a factor of two than the average. The 10.8 cm solar flux during this time was at the maximum of the 27 day cycle with values of 90 ± 2 and while variations in the solar flux did correspond to variations in the N_2 concentrations,

the larger variations in concentrations were associated with changes in magnetic activity. The data thus seem to indicate a rather strong sensitivity of the N_2 concentrations to magnetic conditions. Pass 182 BP, in particular, shows an N_2 concentration of four times that of the average value for an altitude of 430 kilometers. This behavior is in general qualitative agreement with the results of the pressure gage experiments on Explorer XVII. It should be pointed out that all the N_2 data used in this figure and for this discussion are from middle to high latitude passes in the Northern Hemisphere. All of the nighttime data being discussed here, including O and He, were obtained between 3 April and 22 April 1963.

4.2 Nighttime Atomic Oxygen

The nighttime atomic oxygen concentration variation with altitude is shown in Figure 6. Again ignoring the high A_p passes which occurred on the 14th and 15th of April, it is noted that the "scale height" is consistent with an atmospheric temperature of about 700° with a number density at an altitude of 400 km of $1.0 \pm 0.4 \times 10^7$ atoms per cubic centimeter. As in the case of N_2, the observed changes in concentration with altitude for individual passes should be interpreted as functions of local time and other horizontal effects as well as vertical variations.

It can be seen by comparing Figures 5 and 6 that there is a larger variation between passes in the N_2 concentrations than in the atomic oxygen concentrations. This is a natural consequence of the diffusion phenomena, where, for any constant value $n(z_0)$ in an isothermal region, we have the altitude relationship for a gas component

$$n(z) = n(z_0) \exp\left(-\frac{m\bar{g}\, z}{kT}\right)$$

where $\bar{g}$ is an average gravitational acceleration over the altitude range z_0 to z_1 and $z = z_1 - z_0 > 0$. For a temperature variation from T_1 to T_2 one obtains

$$\frac{\Delta n}{n} = \frac{m\bar{g}\, z}{T_1\, T_2}\,\Delta T.$$

Thus, at any altitude $z > z_0$, a change in temperature ΔT will change the concentration of N_2 (mass 28) more than it will affect the concentration of 0 (mass 16) in the ratio of the masses 28/16 = 1.75. This is, of course, only an approximation to the behavior for a change in exospheric temperature as the value of the temperature gradient in the thermosphere also plays a large part in the concentrations at higher altitudes. For instance in a diffusive model at an altitude of 400 kilometers the ratio of the concentration change for $T_1 = 650°$, $\Delta T = 50°$ is 2.04/1.45 = 1.41 and for $\Delta T = 100°$ this ratio is 3.70/1.98 = 1.87. This approximate relationship does however emphasize the fact that heavier mass components will exhibit a larger variation in concentration for a given temperature change than will light components.

Further comparison of the N_2 and 0 concentrations shows that they are both about 1×10^8 cm^{-3} near 300 km (C. Reber, 1964)[27]. Since rocket measurements indicate that the ratio $n(N_2)/n(0)$ is also unity near 200 km (A. O. Nier, et al, 1964)[28], there must be a thick region (which is a transition region) where N_2 and O, being of the same order,

will vary in a very complex way due to the diurnal variations of temperature. Diffusive conditions must be such that the time required to reach equilibrium is long.

4.3 Nighttime Helium

The helium data, shown in Figure 8 have sufficient scatter (due possibly to the low signal to noise) that it is difficult to do more than indicate rather gross variations and trends. One of these is the difference between the observations above 600 km altitude obtained in the Southern Hemisphere and those below 550 km from the Northern Hemisphere. The altitude variations of the data from the two hemispheres appear to be consistent with atmospheric temperatures of approximately 700° but the northern (springtime) data appear to be about 50% lower than that from the south (fall hemisphere). This is not surprising in itself as the concentration of helium in the heterosphere is believed to be extremely sensitive to the height of the level where diffusion begins to predominate over mixing: an increase of 5 kilometers in the height of the diffusion level may be associated with a decrease by a factor of two in the concentration of helium above 200 kilometers for the same atmospheric temperature (M. Nicolet, 1961)[18]. Furthermore, the altitude for the diffusion level is expected to be seasonally dependent.

Comparing the nighttime atomic oxygen data to the helium data, it can be seen that the concentrations of the two species become comparable near 550 kilometers in the Northern Hemisphere. The two Quito passes, 183 and 242 show helium having a higher concentration than atomic oxygen at 650 kilometers.

4.4 Nighttime Mean Mass and Total Mass Density

The nighttime mass density data are shown in Figure 8. It can be seen that the total density in the northern latitudes ranges between $8 \pm 2 \times 10^{-15}$ gm cm^{-3} at 300 kilometers and $1.4 \pm 0.6 \times 10^{-16}$ gm cm^{-3} at 450 kilometers altitude. There were, unfortunately, no usable nighttime data at altitudes less than 300 kilometers.

In comparing these data to the simultaneous pressure gage measurements on Explorer XVII nearly all the densities fall within the limits of error claimed for one or the other of the two experiments (G. P. Newton, et al, 1965)[15]. In general the pressure gages indicate densities which are lower than those from the mass spectrometer, with a difference of less than 40% for most comparisons.

If one makes a simple extrapolation of the lower altitude data from 300 kilometers down to 270 kilometers, a comparison becomes possible with densities deduced from satellite drag data for Explorer XVII. Upon making this extrapolation, using all the low altitude passes, a value at 270 km is obtained of $2.5 \pm 1.0 \times 10^{-14}$ gm cm^{-3} for the period 6 April to 20 April. By ignoring those passes which correspond to periods of increased magnetic activity, 163 WNK, 237 WNK and 254 NFL, we arrive at a lower value for 270 km of approximately $1.8 \pm 0.3 \times 10^{-14}$ gm cm^{-3}. This can be compared to a value obtained from drag data by Slowey (J. Slowey, 1964)[29] for the same period and altitude of $3.2 \pm 1.1 \times 10^{-14}$ gm cm^{-3}. It might be pointed out that in the discussion of drag results by Slowey the Nicolet model for a temperature of 773° is used and the

resulting density is quoted as being too high. The temperature range deduced by Slowey is 635° (Explorer XVII drag) to 704° (solar flux $F_{10.7} = 81$) so the densities should be referenced to a lower model temperature.

Figure 9 presents the mean mass as a function of altitude. For altitudes greater than 425 kilometers the mean mass is generally less than 16 for low solar and magnetic activity reflecting the importance of helium. The majority of these data were obtained in the time interval between 23.00 hours and 3.00 hours and from many Northern Hemisphere locations with spread in latitude of greater than 30°. It should also be kept in mind, of course, that the concentration of hydrogen is not included in these mean mass data.

4.5 Daytime Molecular Nitrogen

If there is any one outstanding characteristic of the results of the daytime N_2 measurements, it is the extreme variability of the concentration over the two month period of observation (Figure 10). As the greatest number of measurements were made near perigee (258 km), this altitude presented the highest probability of seeing variations. This was in fact borne out, as ten measurements between 260 and 265 kilometers displayed a variation of nearly a decade.

Between 21 May and 31 May, the local time of the perigee measurements ranged between 12.70 hours and 10.30 hours and the N_2 concentration at 265 kilometers varied from 8.0×10^7 cm^{-3} to 6.6×10^8 cm^{-3}.

Apparently values near 1.0 - 2.0 $\times 10^8$ cm^{-3} are representative of average undisturbed conditions as the higher values (e.g. 831 BP, 846 BP and 876 BP) followed closely a magnetic disturbance of $A_p = 21$.

An interesting sidelight to this is that for these particular passes which indicate a higher N_2 density the positive ion density, as measured by one of the Explorer XVII electrostatic probes, is lower than for corresponding measurements on magnetically quiet days (L. H. Brace, et al, 1965)[16]. This is to be expected when one considers that molecular nitrogen plays an important role in the loss mechanism for electrons in the F-region (J. W. Wright, 1964)[30]. The lower values of N_2 density were observed at times when A_p was no greater than 4 and averaged about 3. The values at 260 kilometers corresponding to relatively undisturbed conditions agree quite closely with values obtained by Nier (A. O. Nier, et al, 1964)[28], (A. E. Hedin, et al, 1964)[31], (H. E. Hinteregger, et al, 1964)[32], (N. W. Spencer, et al, 1965)[24] from rocket flights in the first part of 1963. (We obtained Nier's value at 260 kilometers by extrapolating his measured data upward with a diffusive model for a temperature of 800°). These rocket measurements indicate concentrations for N_2 at 260 kilometers of 1.5 to 2.0 $\times 10^8$ cm^{-3}. Pokhunkov's measurement of November 1961 indicated a value of 1.1 $\times 10^9$ cm^{-3} for this same altitude and corresponded to a higher level of the solar cycle (A. A. Pokhunkov, 1963)[5].

As the observations in May moved to higher altitudes in the Northern Hemisphere, the times of observation became earlier in the day until we

approached sunrise measurements at 500 kilometers (see Figure 4). The decrease of the N_2 concentration with altitude is consistent with an atmospheric temperature of 825° ± 75°K throughout this morning measurement period.

The measurements in early April, all near the perigee altitude, indicate a number density of 1.6 - 3.0 × 10^8 cm^{-3} at 260 kilometers. These passes occurred late in the day, 197 COL being as late as 21.47 hours. 197 COL, a relatively high density measurement, also followed by two days a minor magnetic storm of A_p = 17.

At the 350 kilometer level, there were a number of passes (772, 728, and 743 COL) around 7.50 hours to 8.50 hours prior to 24 May which indicate a concentration of 7.5 × 10^6 cm^{-3}. On and following the 25th of May, there is a continuation of this group of passes (787, 802, and 817 COL), but now the concentration is about 1.6 × 10^7 or more than a factor of two increase. At the time of this increase, the 10.7 cm flux increased from 89 to 93 and the A_p index increased from 2 to 8, indicating again the sensitivity of the N_2 concentration to modest changes in magnetic and solar conditions. Also, the higher concentration persisted at least through 27 May, while the solar 10.7 cm index dropped to 76 and the A_p oscillated between 6 and 7, indicating perhaps a stronger sensitivity to A_p than to $F_{10.7}$ for values of these magnitudes.

Shown also in Figure 10 are the results from six Southern Hemisphere passes between 12.00 hours and 15.00 hours. These show a

considerable variation in the N_2 concentrations, indicating either a difference in local temperatures or in the boundary conditions at lower levels, or, more likely, differences in both.

4.6 Daytime Atomic Oxygen

The daytime atomic oxygen data shown in Figures 11 and 12 were obtained during early April and late May in both the Northern and Southern Hemispheres. The April data, Figure 11, are entirely from the Northern Hemisphere (with the exception of 13 QUI which extends to -5.3°), while the May data shown in Figure 12 include both Northern and Southern Hemisphere results.

The lowest altitude data shown in Figure 10, from 258 km to 300 km, were obtained at local times around sunset. It is seen that the concentration of atomic oxygen near 260 km is $2.0 - 2.7 \times 10^8$ cm^{-3} which is comparable to that for molecular nitrogen measured at the same time. The general altitude variation from 260 km up is consistent with a temperature of about 800°.

At higher altitudes, the data taken near sunrise indicate number densities of $1.6 \pm 0.4 \times 10^6$ cm^{-3} at 500 km in the Northern Hemisphere. An early evening pass from Quito indicates a concentration of 1.6×10^7 cm^{-3} at 375 kilometers and a sunrise Quito pass at 675 kilometers shows 1×10^5 cm^{-3}. If the Northern data are interpreted in terms of an isothermal diffusive atmosphere, it appears that the sunrise atomic oxygen measurements indicate a temperature as high as the sunset measurements indicate, implying a quite rapid response to the solar energy input.

Also, since the sunrise data are entirely from above 450 kilometers altitude, a rapid response would be expected due to the low number density. The concentration at 450 km is only about 0.01 that at perigee so the time required to establish equilibrium at the higher altitude would also be 0.01 that required at 260 kilometers.

The data acquired from 20 May to 31 May, Figure 12, include Northern and Southern Hemisphere measurements up to 600 kilometers altitude and ranges from near sunrise to mid-afternoon. At perigee there are concentrations from 9×10^7 cm^{-3} (724 WNK) to 2.5×10^8 cm^{-3} (817 FTM) at noon time, emphasizing again the large variations encountered. The O/N_2 ratios on magnetically undisturbed days typically range between 1.0 and 1.6, with two examples (753 WNK and 118 BP) greater by an order of magnitude. These data imply an O/N_2 ratio of unity between 200 km and 250 km, in agreement with rocket measurements. At altitudes greater than 450 kilometers it is noted that the Southern Hemisphere passes show a generally higher oxygen concentration than the Northern passes by about a factor of five; the Southern passes are mid-afternoon measurements while the Northern observations were generally made in the early-to-mid-morning.

4.7 Daytime Helium

Figures 13 and 14 show the results of the helium measurements up to 735 kilometers; Figure 13 contains the data obtained in April at northern latitudes and near the equator, while Figure 14 presents the May data, northern, southern and equatorial.

At 260 kilometers in April the data show helium concentrations of about $1.4 \pm 0.3 \times 10^6$ cm^{-3} at local times near sunset in the Northern Hemisphere. At 500 kilometers around sunrise, this concentration falls to $4.5 \pm 1.5 \times 10^5$ cm^{-3}. It is seen that this decrease with altitude is generally consistent with a temperature of 800°.

The equatorial passes at high altitudes near sunrise indicate a generally higher number density for helium than is obtained at higher latitudes. If the concentrations obtained at altitudes near 700 kilometers at the equator are the result of an isothermal diffusive atmosphere, then the concentrations here appear to be about 2.5 times the concentrations farther north. There must be some effect other than just a change in atmospheric temperature to cause this difference in the concentration as helium is relatively insensitive to temperature variations. For example, a change from 800° to 1000° would produce an increase of only 1.6 at 700 kilometers. This is not enough to explain the differences observed.

The same sort of behavior is observed when comparing data obtained in the latter part of May: the helium densities in the Southern Hemisphere are about 3.5 times those obtained at northern latitudes. Equatorial densities, passes 803 and 877 QUI, in this case fall between those obtained in the Northern and Southern Hemispheres.

Examination of the perigee data again points up a rather large variation between 21 May and 31 May, as with the N_2 and O data. In the case of helium, however, there is a different trend, as those passes which

exhibited the highest densities for N_2 and O, 831 BP, 846 BP and 876 BP, are among the lowest for helium concentrations. This would imply differing sensitivities for the different species to the various mechanisms which lead to changes in number densities above the thermosphere.

By comparing the daytime helium altitude behavior with that of atomic oxygen, Figures 11, 12, 13 and 14, it can be seen that a He/O ratio of unity is attained near 600 kilometers for both Northern and Southern Hemispheres, in April and May.

4.8 Daytime Mean Mass and Total Density

The total density follows, naturally, the variations in the concentrations of the major components from which it was deduced. The calculation of this quantity and its presentation as a function of altitude (Figure 15) are advantageous, however, as a means of comparison with other experiments and with drag calculations, as was done in Section 3.5.

Thus, we note that the daytime densities calculated for April (about 20.00 hours) are 1.5 to 2.2×10^{-14} gm cm^{-3} at an altitude near 260 kilometers. For the same time and altitude, the drag densities are quoted as 3.16 to 3.31×10^{-14} gm cm^{-3} (J. Slowey, 1964)[29]. In May, the perigee densities from the mass spectrometer range from about 6.4×10^{-15} gm cm^{-3} to 4×10^{-14} gm cm^{-3}, with the undisturbed conditions falling generally less than 2.5×10^{-14} gm cm^{-3}. This can be compared to 3.80 to 4.79×10^{-14} gm cm^{-3} for the drag results at the same altitude. It appears that for the passes involved there is a systematic difference

of 30% to 50%, with the drag densities showing up higher than the direct measurements.

At 450 kilometers, a variation of a decade is seen between the densities in the Northern Hemisphere early in the morning and those in the Southern Hemisphere around noon one week later. It should be noted also that a magnetic storm occurred prior to the Southern Hemisphere passes, a storm which apparently caused a factor of three increase in density at perigee in this same time period. Thus, the variation at 450 kilometers should not all be attributed to the difference in location and local time.

The mean mass at perigee for the period around this same magnetic storm is interesting from the standpoint of the large increase exhibited (Figure 16). A comparison of the gas concentrations involved shows an increase in atomic oxygen of about 2.5, while molecular nitrogen varies by more than a factor of 6. The ratio of the variations of 0 and N_2 is 6/2.5 = 2.4 while ratio of 1.55/1.22 = 1.27 is expected for a temperature difference of 100° from 700° to 800° from a diffusive model. Thus the difference in the variation of 0 and N_2 is more than expected on the basis of diffusive models for a change in temperature and must be due to changes in the conditions near the diffusive level. It should be noted that this ratio in the variations of atomic oxygen and molecular nitrogen also applies to the variation of the $n(N_2)/n(0)$ ratio; i.e.

$$\frac{n(N_2)_1}{n(N_2)_2} \Big/ \frac{n(0)_1}{n(0)_2} = \frac{n(N_2)_1}{n(0)_1} \Big/ \frac{n(N_2)_2}{n(0)_2}.$$

Thus the $n(0)/n(N_2)$ ratio has varied by a factor of 2.4 over this same time interval of one week. Variations of this magnitude (or larger) would probably explain many of the apparent "inconsistencies" between results of rocket experiments in the past where the time interval between measurements has been months, and sometimes years.

4.9 Dynamic Effects

Due to the high velocity of the satellite, the difference in local sun time between measurements of a gas concentration made on a satellite pass may be as much as an hour, although the real time difference is only one minute. This effect, combined with a possible variation in latitude of 5° or more between data points, serves to locate these measurements in sometimes widely differing environments. As stressed earlier, in those instances where there is a relatively large variation in atmospheric parameters with time and location, the results of a pair of measurements at different altitudes will bear only a complicated relationship to an instantaneous vertical profile at either measurement location.

This dynamic effect has shown up most noticeably in satellite passes around sunrise and especially at northern latitudes, most probably due to the sequence of measurement parameters within a pass in this region. Figure 17 shows the variation of "scale height", H, with local time for those passes where there is a significant difference in altitude between measurements. The "scale height" here is calculated by taking the two measurement altitudes, z_0 and z_1, along with the corresponding number densities, n_0 and n_1, and using

$$\mathcal{H} = \frac{z_1 - z_0}{\ln n_0/n_1}.$$

It can be seen that between 4.00 and 8.00 hours $\mathcal{H}(N_2)$ goes through a large maximum, while $\mathcal{H}(0)$ exhibits a smaller maximum. There are even a number of passes between 5.00 and 6.00 hours where $\mathcal{H}(N_2)$ becomes negative, i.e. increasing concentration with altitude.

Examining the altitude/latitude/time relationships for these unusual passes brings out one pertinent point: the higher altitude point is considerably closer in time to a local "high altitude sunrise" (J. Lugeon, 1957)[33] than the lower altitude measurement. The other, more normal appearing measurements, were obtained in such a way as to place both points about the same time interval after the upper atmospheric sunrise. Also, the locations and dates for these passes put them very close to the point where the sun never actually "sets". At 550 kilometers altitude, the sun never went below the horizon at latitudes above 46° in the latter part of May, while the measurements were made from 35° to 47° latitude and in the altitude range 465 kilometers to 540 kilometers. This would indicate a constant source of energy into the atmosphere very near to where the measurements were made. Any explanation of these observations must include a relatively rapid reaction of the atmosphere to the solar energy input at altitudes greater than 400 kilometers, as well as horizontal gradients and mass transport near sunrise.

5. CONCLUSIONS

It has been shown that direct measurements of atmospheric composition are possible from a high altitude earth orbiting satellite. The results of these measurements compare favorably with results from pressure gage experiments on the same spacecraft as well as satellite drag data and direct measurements made from rockets. The satellite measurements offer greatly increased coverage, both altitude and location, and can be used to infer local time variations at specific altitudes.

This increased coverage inherent with a satellite brings its own peculiarities to bear on the problem of investigation of upper atmosphere phenomena. Chief among these is the large variation in geographic location and local time for a given altitude change, so that the data cannot usually be interpreted in terms of a simple altitude profile of concentration. We see, for example, data showing molecular nitrogen and atomic oxygen behavior at night (Section 4.1 and 4.2) which, if interpreted in terms of a variation with altitude alone would imply a lack of thermal equilibrium between these two species. A much more plausible explanation would include variations in the boundary conditions at lower levels as a function of location and/or time and horizontal gradients in the concentrations of the two species involved.

The daytime measurements indicate that average conditions near 260 kilometers were an N_2 concentration of $1.5 \pm 0.5 \times 10^8$ cm^{-3}, O concentration of $2.0 \pm 0.5 \times 10^8$ cm^{-3} and a He concentration of $1.4 \pm 0.3 \times 10^6$ cm^{-3}. Observations of the O/N_2 ratio during undisturbed

conditions at this altitude indicate that a ratio of unity would be reached between 200 km and 250 km. Altitude variations of concentrations are consistent with an atmosphere in diffusive equilibrium at a temperature of 825 ± 75°K.

The night measurements in general are consistent with an isothermal atmosphere at a temperature of 650° to 700°K. Average, undisturbed conditions at an altitude of 400 kilometers in the Northern Hemisphere appear to be an atomic oxygen concentration of $1.0 \pm 0.4 \times 10^{7}$ cm^{-3}; molecular nitrogen concentration of $2.0 \pm 1.0 \times 10^{6}$ cm^{-3}; and helium concentration of $6.0 \pm 2.0 \times 10^{5}$ cm^{-3}. These individual particle densities combine to yield a total density under the same conditions of $3.5 \pm 1.0 \times 10^{-16}$ gm cm^{-3}. The ratio of N_2 and 0 is near unity at 300 kilometers in these nighttime measurements implying a rather thick transition region from an N_2 atmosphere to the altitude where atomic oxygen becomes dominant. Above about 550 kilometers, helium has a higher concentration than oxygen.

A somewhat unexpected result of the observations was the large variability of the absolute concentrations and ratios of concentrations of the components measured at the same altitudes and local times (and, it might be emphasized, with the same piece of measuring equipment) on successive days. There is a strong sensitivity to changes in magnetic activity, especially for the heavier particles. Some of these variations cannot be explained entirely on the basis of temperature changes in the upper atmosphere, but must be attributed to changes in the boundary conditions at the base of the diffusive atmosphere (homopause). Further

investigations are clearly required in order to define the source of these variations and their relations to the various energy inputs to the atmosphere.

REFERENCES

1. J. W. Townsend, E. B. Meadows and E. C. Pressly, Rocket Exploration of the Upper Atmosphere, R. L. F. Boyd and M. J. Seaton (Editors), Pergamon, London (1964).

2. J. W. Townsend and E. B. Meadows, Annales de Geophysique, 14, 117 (1958).

3. E. B. Meadows and J. W. Townsend, Annales de Geophysique, 14, 80 (1958).

4. A. O. Nier, J. H. Hoffman, C. Y. Johnson, and J. C. Holmes, J. Geophys. Res., 69, 979 (1964).

5. A. A. Pokhunkov, Kosmicheskiye Issledovaniya, 1, 147 (1963).

6. E. Meadows-Reed and C. R. Smith, J. Geophys. Res., 69, 3199 (1964).

7. E. J. Schaefer and M. H. Nichols, Space Research IV, Amsterdam (1963).

8. D. R. Taeusch, G. R. Carignan and H. B. Niemann, Univ. of Michigan, College of Engineering Scientific Report MS-3.

9. L. M. Jones, Rocket Exploration of the Upper Atmosphere, R. L. F. Boyd and M. J. Seaton (Editors), Pergamon, London (1954).

10. G. V. Groves, Proc. of the Royal Society, 263, 212 (1961).

11. R. Jastrow and R. Bryant, J. Geophys. Res., 65, 3512 (1960).

12. L. G. Jacchia, Rev. of Modern Physics, 35, 973 (1963).

13. H. K. Paetzold, J. Atmosph. and Terr. Physics, 16, 259 (1959).

14. D. G. King-Hele and D. M. C. Walker, Space Research II, Amsterdam, 918 (1961).

15. G. P. Newton, R. Horowitz and W. Priester, Planet. Space Sci., (in this issue) (1965).

16. L. H. Brace, N. W. Spencer and A. Dalgarno, Planet. Space Sci. (in this issue) (1965).

17. M. Nicolet, Planet. Space Sci., 5, 1 (1961).

18. M. Nicolet, Space Research II, Amsterdam (1961).

19. N. W. Spencer, Planet. Space Sci., (in this issue) (1965).

20. E. B. Meadows, Eighth Annual Meeting of ASTM Committee E-14 on Mass Spectroscopy (1960).

21. L. G. Hall, P. F. Howden and T. F. Iwasaki, Eighth Annual Meeting of ASTM Committee E-14 on Mass Spectroscopy (1960).

22. N. W. Spencer and C. A. Reber, Space Research III, Amsterdam (1963).

23. C. A. Reber and L. G. Hall, submitted to Rev. Sci. Inst. (1965).

24. N. W. Spencer, L. H. Brace, G. R. Carignan, D. R. Taeusch and H. Niemann, submitted to J. Geophys. Res. (1965).

25. W. L. Fite and R. T. Brackman, Phys. Rev., 113, 815 (1959).

26. R. Horowitz and H. E. LaGow, J. Geophys. Res., 62, 57 (1957).

27. C. Reber, J. Geophys. Res., 69, 4681 (1964).

28. A. O. Nier, J. H. Hoffman, C. Y. Johnson and J. C. Holmes, J. Geophys. Res., 69, 979 (1964).

29. J. Slowey, Smithsonian Astrophysical Observatory Special Report, No. 157, (1964).

30. J. W. Wright, Electron Density Distribution in Ionosphere and Exosphere, E. Thrane (Editor) North Holland (1964) pp. 186-198.

31. A. E. Hedin, C. P. Avery and C. D. Tschetter, J. Geophys. Res., 69, 4637 (1964).

32. H. E. Hinteregger, L. A. Hall and G. Schmidtke, presented at Fifth International COSPAR Meeting, Florence (1964).

33. J. Lugeon, Tables Crepusculares (Twilight Tables), Academie Polonaise des Sciences (1957).

FIGURES

Figure 1 – The Explorer XVII Mass Spectrometer, showing the ion source (where the neutral particles are ionized by electron bombardment), the electrostatic ion lens, the electric sector and the magnetic analyzing region. The relationship between the spectrometer axis (which is the same as the satellite spin axis) and the velocities of the incoming particles (anti-parallel to the satellite velocity vector) is also shown.

Figure 2 – Photograph of a portion of a telemetry record showing the logarithmic amplifier output for one pass. Each mass is sampled for eight seconds, four in high sensitivity and four seconds in low sensitivity. The precision of the telemetry system is 0.2%.

Figure 3 – The relationships $K_j(\alpha)$ relating the measured number density, n_m, for the j^{th} component to the atmospheric number density, n_a, for that component. The angle of attack, α, is the angle between the spectrometer axis and the satellite velocity vector.

Figure 4 – The relationship between the altitude and the local time for those passes discussed in this paper. Each line represents the location of the satellite for approximately one minute of real time.

Figure 5 – The measured number density of molecular nitrogen plotted versus altitude for local times between 21.00 and 4.00 hours. Each point shown is an average of 120 data points over a two second time interval; those measurements taken on one pass, one minute apart, are connected by a straight line. A diffusive model for an atmospheric temperature of 700° is also included for reference.

Figure 6 – The measured number density of atomic oxygen plotted versus altitude for local times between 21.00 and 4.00 hours. Differences in the horizontal position and local time of the satellite between measurements at the same altitude preclude the interpretation of this type presentation as a pure altitude profile. A model profile for T = 700° is also included; the model is reduced in absolute value by a factor of three to avoid confusion with the data points.

Figure 7 – The measured number density of helium plotted versus altitude for local times between 21.00 and 4.00 hours. A diffusive model profile for T = 700° is shown for reference.

Figure 8 – Mass density, $\rho = \Sigma_i n_i m_i$, plotted versus altitude for local times between 21.00 and 4.00 hours. The major components, atomic oxygen, molecular nitrogen and helium, have been included in the summation.

Figure 9 – Mean mass, $M = \Sigma_i n_i M_i / \Sigma_i n_i$, plotted versus altitude for local times between 21.00 and 4.00 hours. The major measured components, N_2, 0 and He have been included in the calculation.

Figure 10 – The measured number density of molecular nitrogen versus altitude for local times between 4.00 and 21.00 hours. A diffusive model profile for T = 800° is included for reference.

Figure 11 – The measured number density of atomic oxygen plotted versus altitude for local times between 4.00 and 21.00 hours. These measurements were made during the first two weeks of April. A diffusive model profile for T = 800° is included for reference.

Figure 12 – The measured number density of atomic oxygen plotted versus altitude for local times between 4.00 and 21.00 hours. These measurements were made during the last two weeks of May. A diffusive model profile for T = 800° is included for reference.

Figure 13 – The measured number density of helium plotted versus altitude for local times between 4.00 and 21.00 hours. These measurements were made in the Northern Hemisphere during the first two weeks in April. A diffusive model profile for T = 800° (reduced in absolute value by a factor of three) is shown for reference.

Figure 14 – The measured number density of helium plotted versus altitude for local times between 4.00 and 21.00 hours. These measurements were made in both the Northern and Southern Hemispheres during the last two weeks in May. A diffusive model profile for T = 800° (reduced in absolute value by three) is shown for reference.

Figure 15 – Mass density, $\rho = \Sigma\, n_i m_i$, plotted versus altitude for local times between 4.00 and 21.00 hours. Only the three major components, N_2, 0, and He, have been included.

Figure 16 – Mean mass, $M = \Sigma\, n_i M_i / \Sigma\, n_i$, plotted versus altitude for local times between 4.00 and 21.00 hours. N_2, 0, and He have been included in the calculation.

Figure 17 – The observed "scale height", $\mathcal{H}$, plotted versus local time. The quantity $\mathcal{H} = z_1 - z_0 / \ln n_0/n_1$ is a measure of the variation in number density with altitude, with the introduction of additional effects due to horizontal changes in the densities of the components.

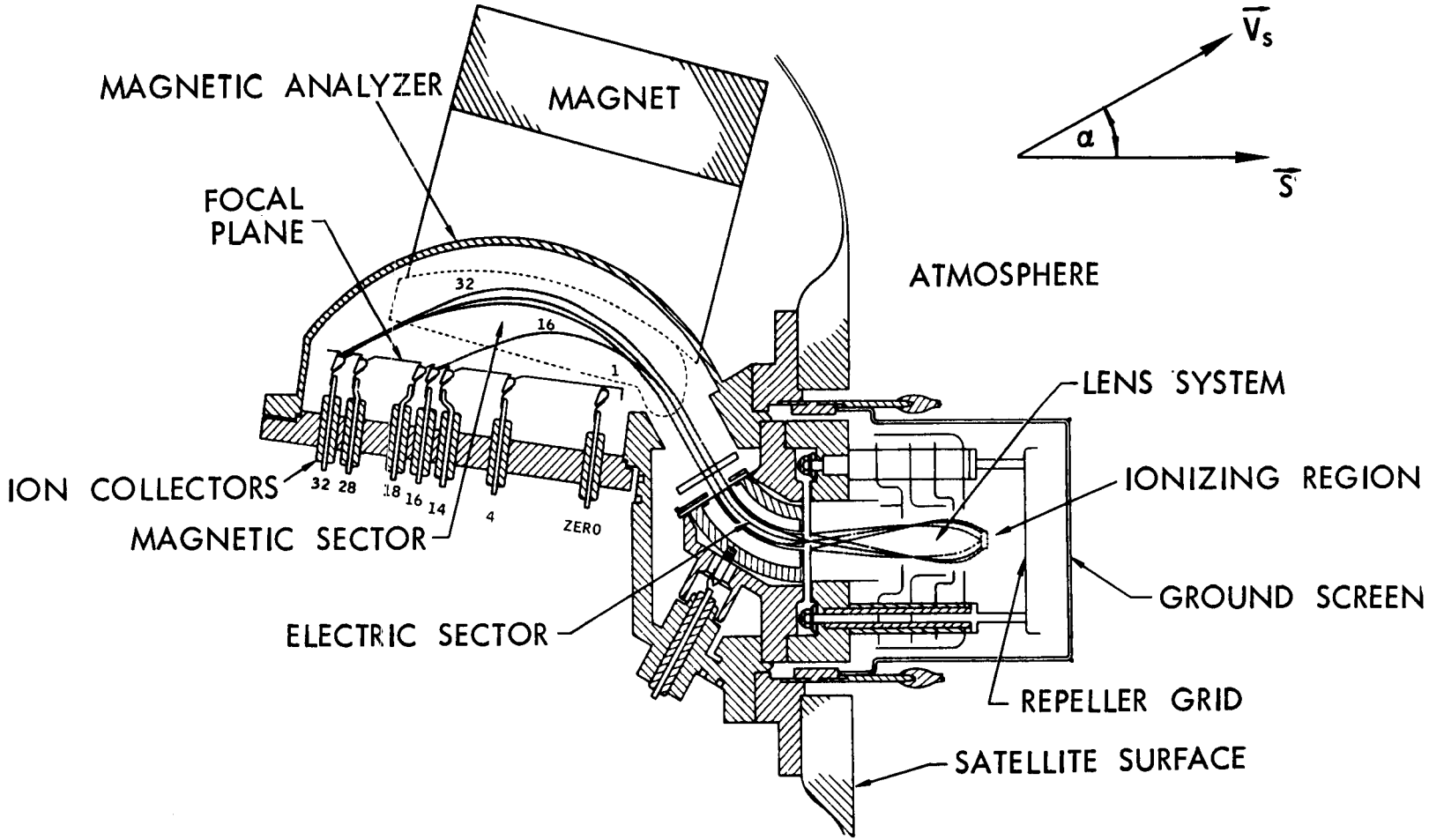
MAGNETIC ANALYZER
MAGNET
FOCAL PLANE
ATMOSPHERE
$\vec{V}_s$
α
$\vec{S}$
32
16
1
LENS SYSTEM
IONIZING REGION
ION COLLECTORS
32 28 18 16 14 4 ZERO
MAGNETIC SECTOR
GROUND SCREEN
ELECTRIC SECTOR
REPELLER GRID
SATELLITE SURFACE

FIGURE 1

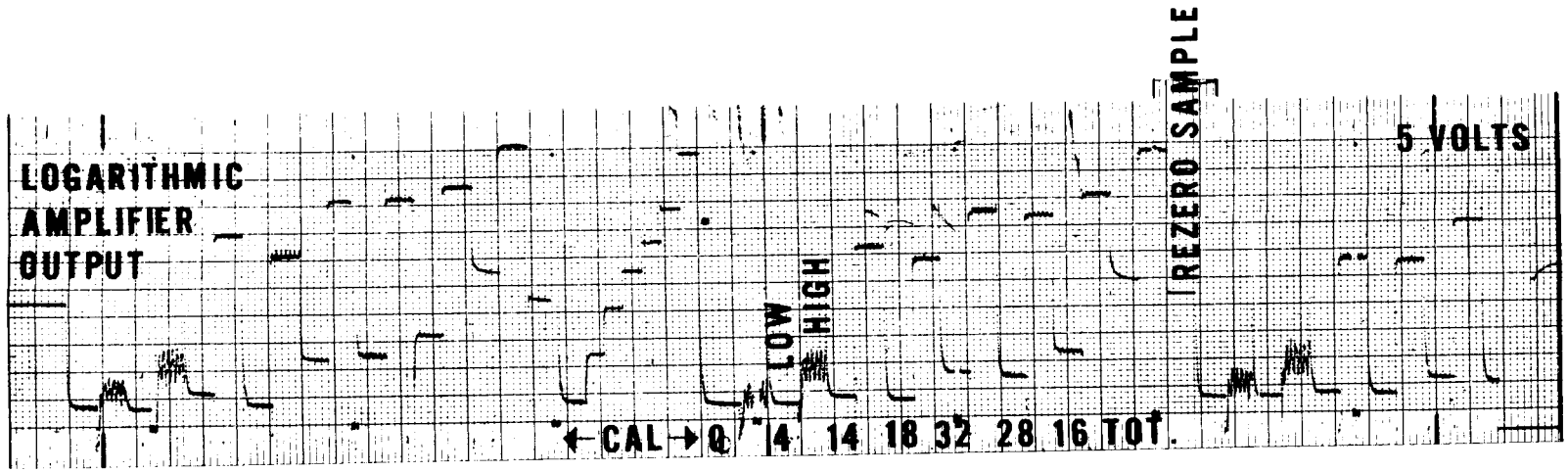
LOGARITHMIC
AMPLIFIER
OUTPUT
5 VOLTS
REZERO SAMPLE
LOW
HIGH
← CAL → 0 4 14 18 32 28 16 TOT.

FIGURE 2

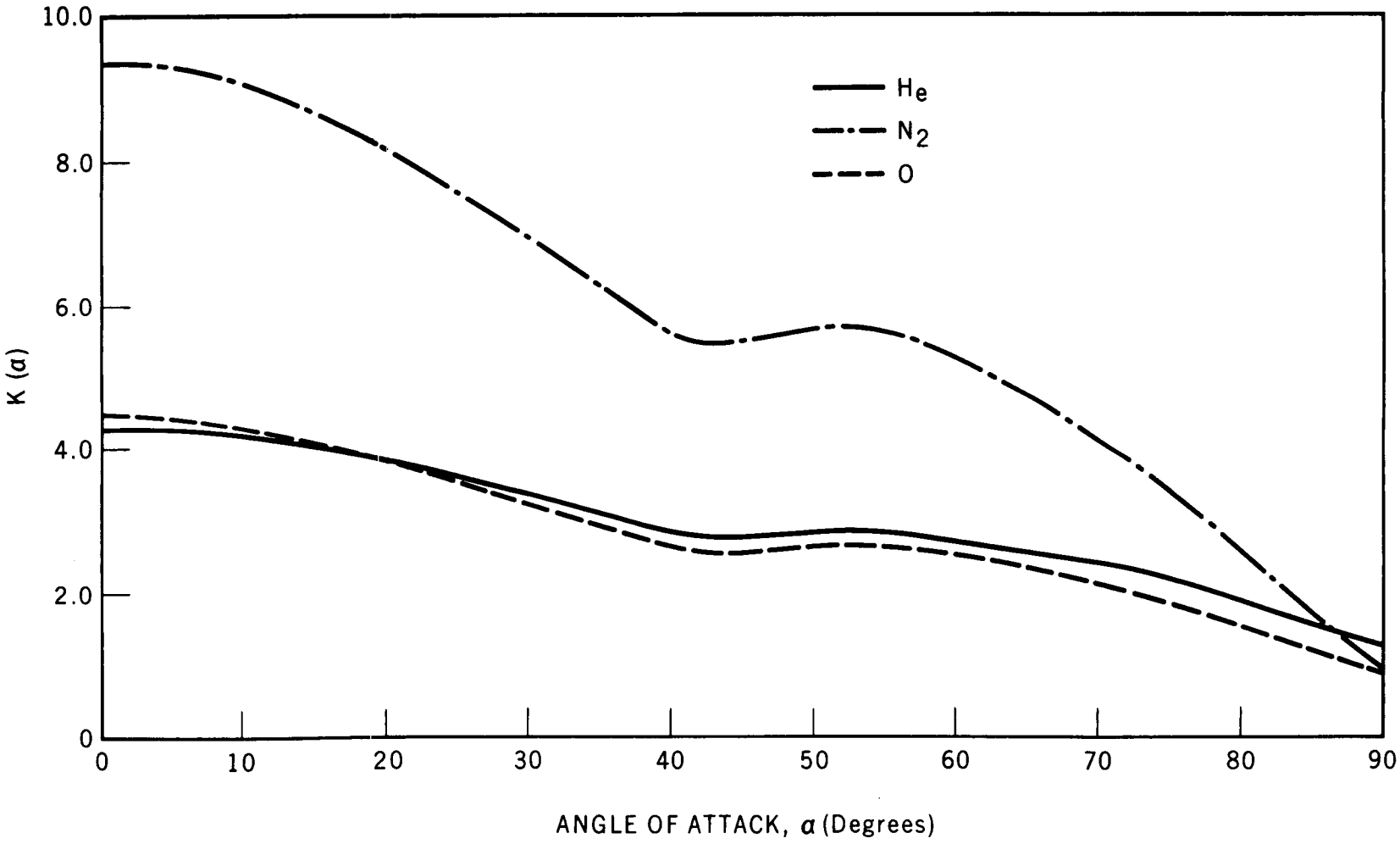
10.0
8.0
6.0
4.0
2.0
0
K (α)
He
N2
O
0
10
20
30
40
50
60
70
80
90
ANGLE OF ATTACK, α (Degrees)

FIGURE 3

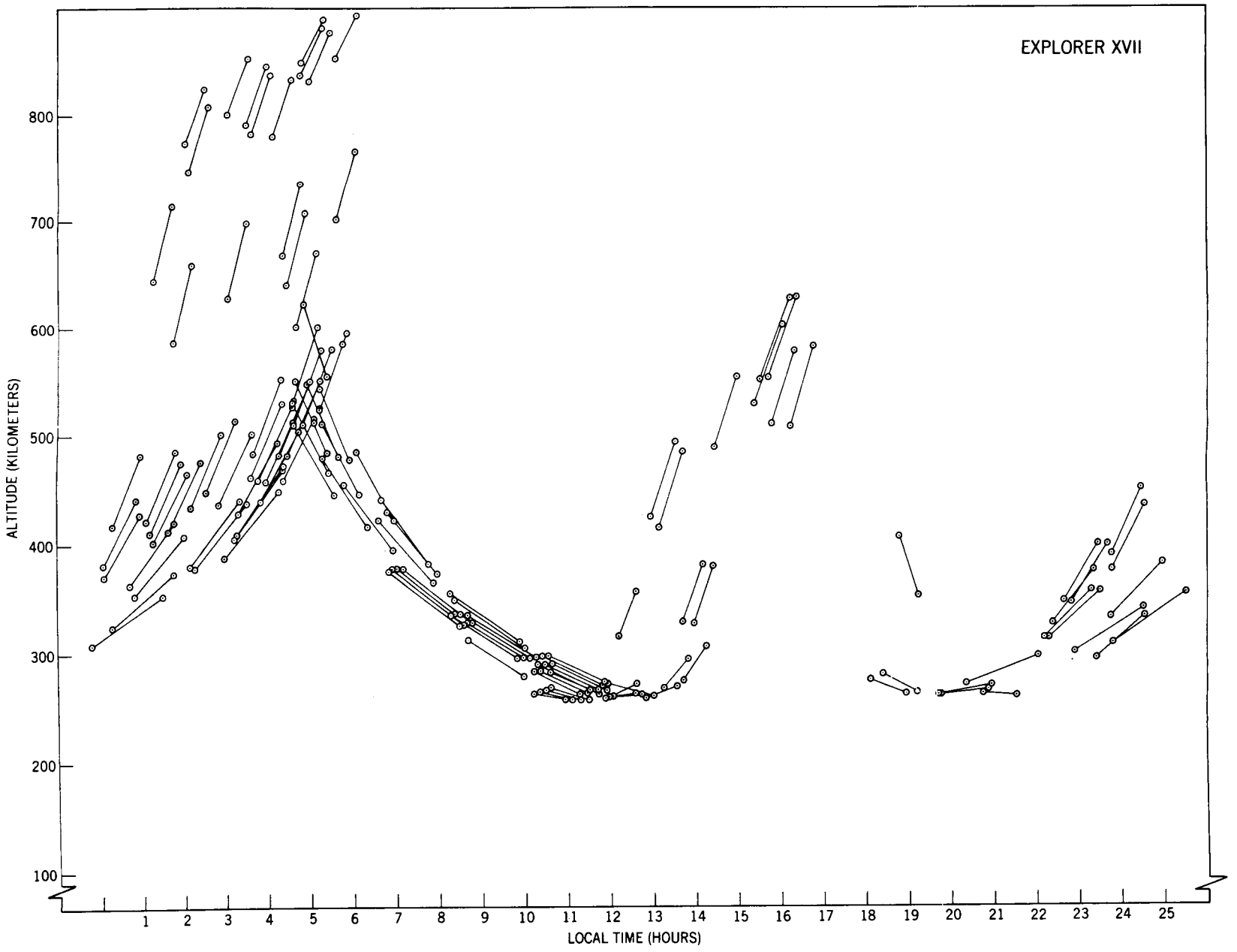
EXPLORER XVII
ALTITUDE (KILOMETERS)
800
700
600
500
400
300
200
100
1 2 3 4 5 6 7 8 9 10 11 12 13 14 15 16 17 18 19 20 21 22 23 24 25
LOCAL TIME (HOURS)

FIGURE 4

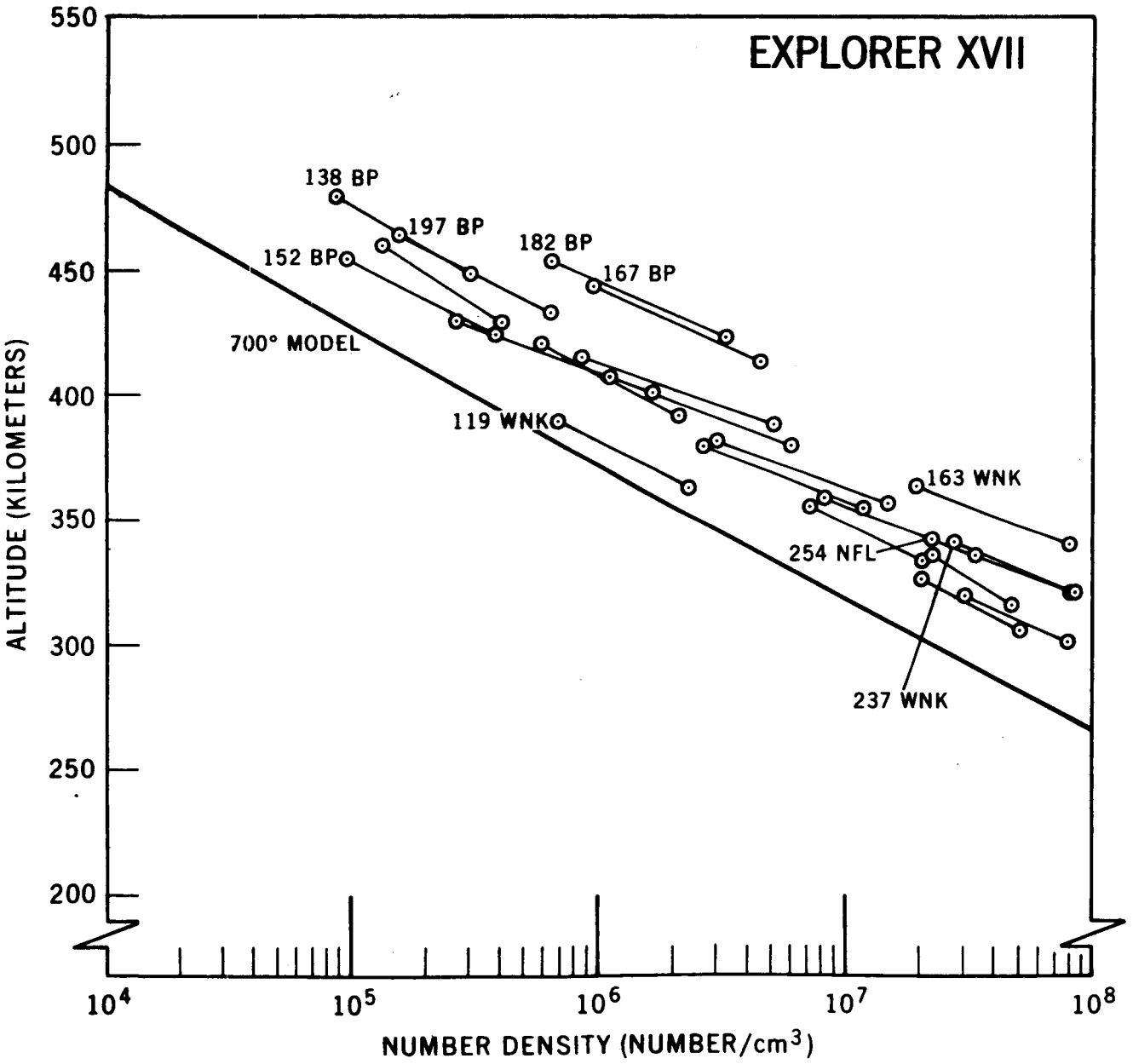
EXPLORER XVII
550
500
450
400
350
300
250
200
ALTITUDE (KILOMETERS)
138 BP
197 BP
182 BP
167 BP
152 BP
700° MODEL
119 WNK
163 WNK
254 NFL
237 WNK
10^4
10^5
10^6
10^7
10^8
NUMBER DENSITY (NUMBER/cm^3)

FIGURE 5

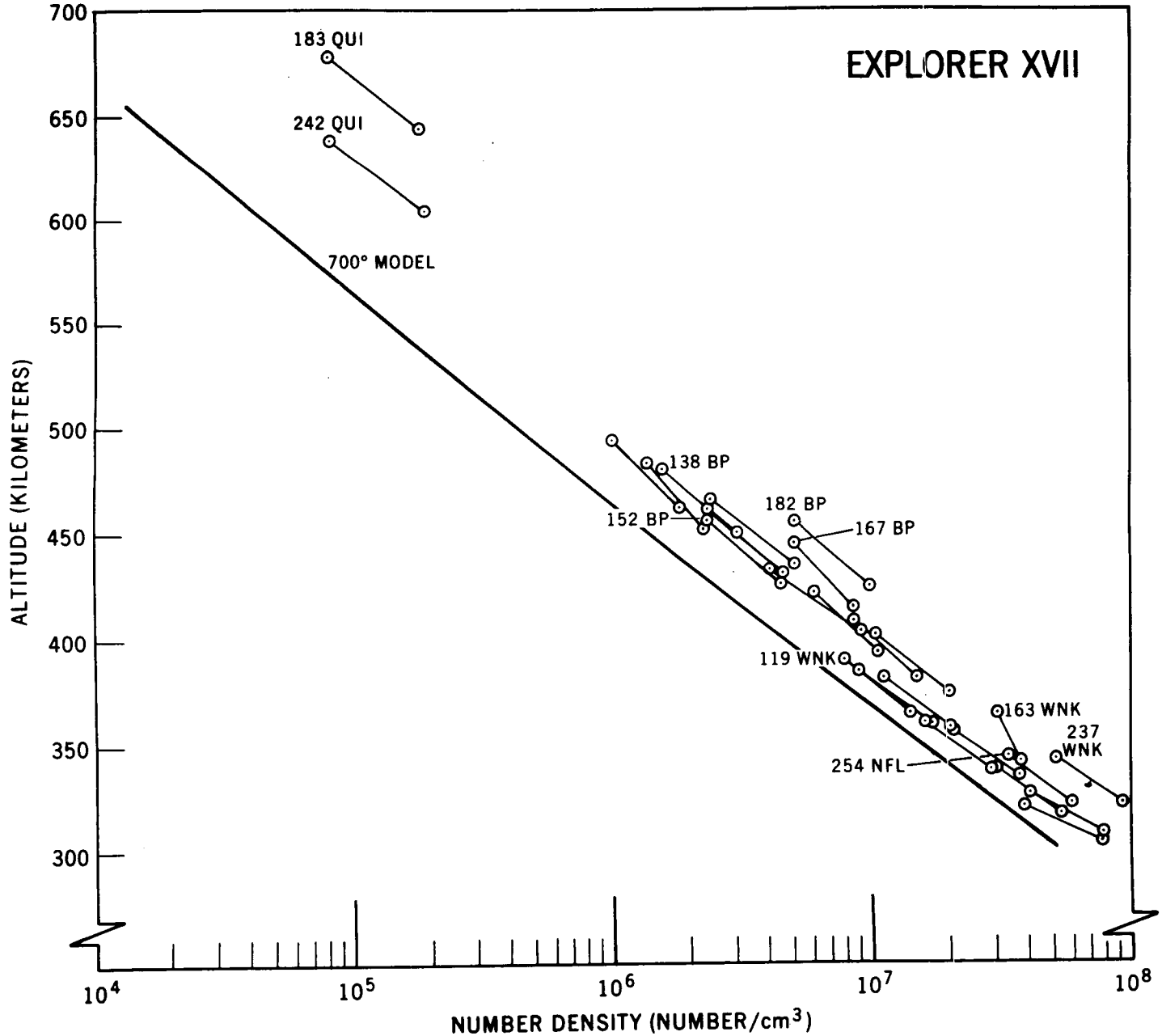
EXPLORER XVII
183 QUI
242 QUI
700° MODEL
138 BP
152 BP
182 BP
167 BP
119 WNK
163 WNK
237 WNK
254 NFL
ALTITUDE (KILOMETERS)
700
650
600
550
500
450
400
350
300
10^4
10^5
10^6
10^7
10^8
NUMBER DENSITY (NUMBER/cm^3)

FIGURE 6

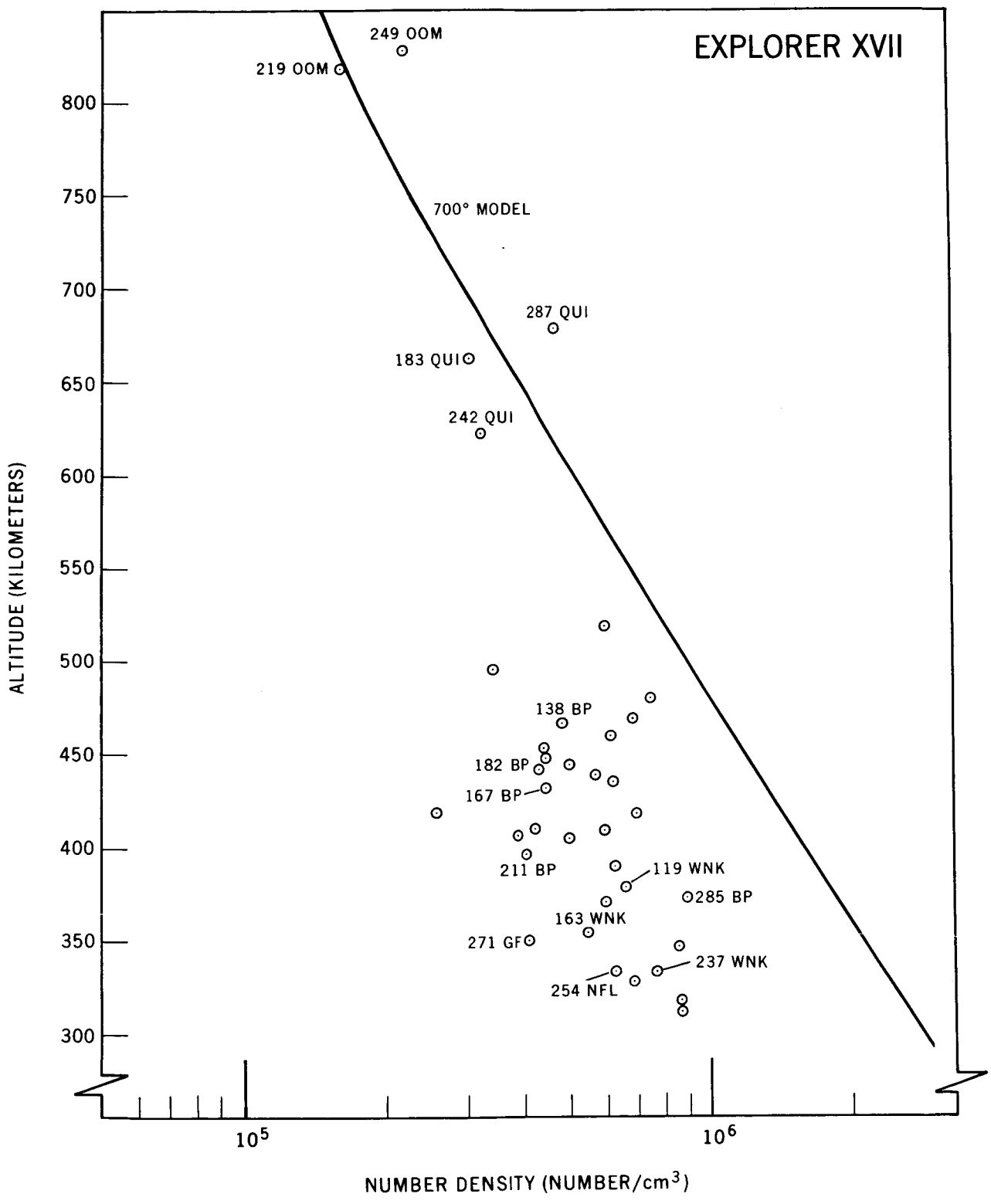
EXPLORER XVII
249 OOM
219 OOM
700° MODEL
287 QUI
183 QUI
242 QUI
138 BP
182 BP
167 BP
211 BP
119 WNK
285 BP
163 WNK
271 GF
237 WNK
254 NFL
800
750
700
650
600
550
500
450
400
350
300
ALTITUDE (KILOMETERS)
10^5
10^6
NUMBER DENSITY (NUMBER/cm^3)

FIGURE 7

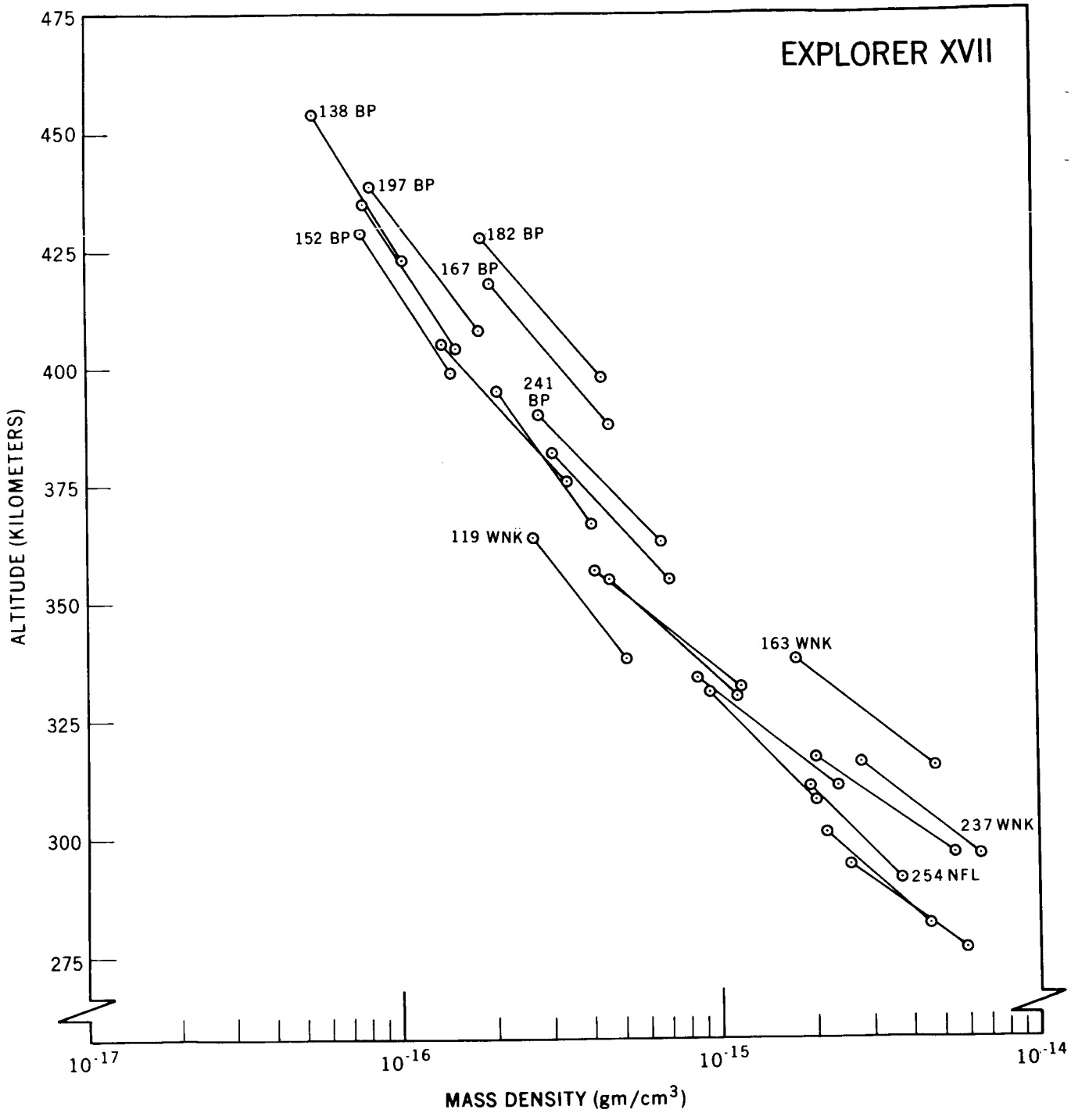
EXPLORER XVII
475
450
425
400
375
350
325
300
275
ALTITUDE (KILOMETERS)
138 BP
197 BP
152 BP
182 BP
167 BP
241 BP
119 WNK
163 WNK
237 WNK
254 NFL
10^{-17}
10^{-16}
10^{-15}
10^{-14}
MASS DENSITY (gm/cm^3)

FIGURE 8

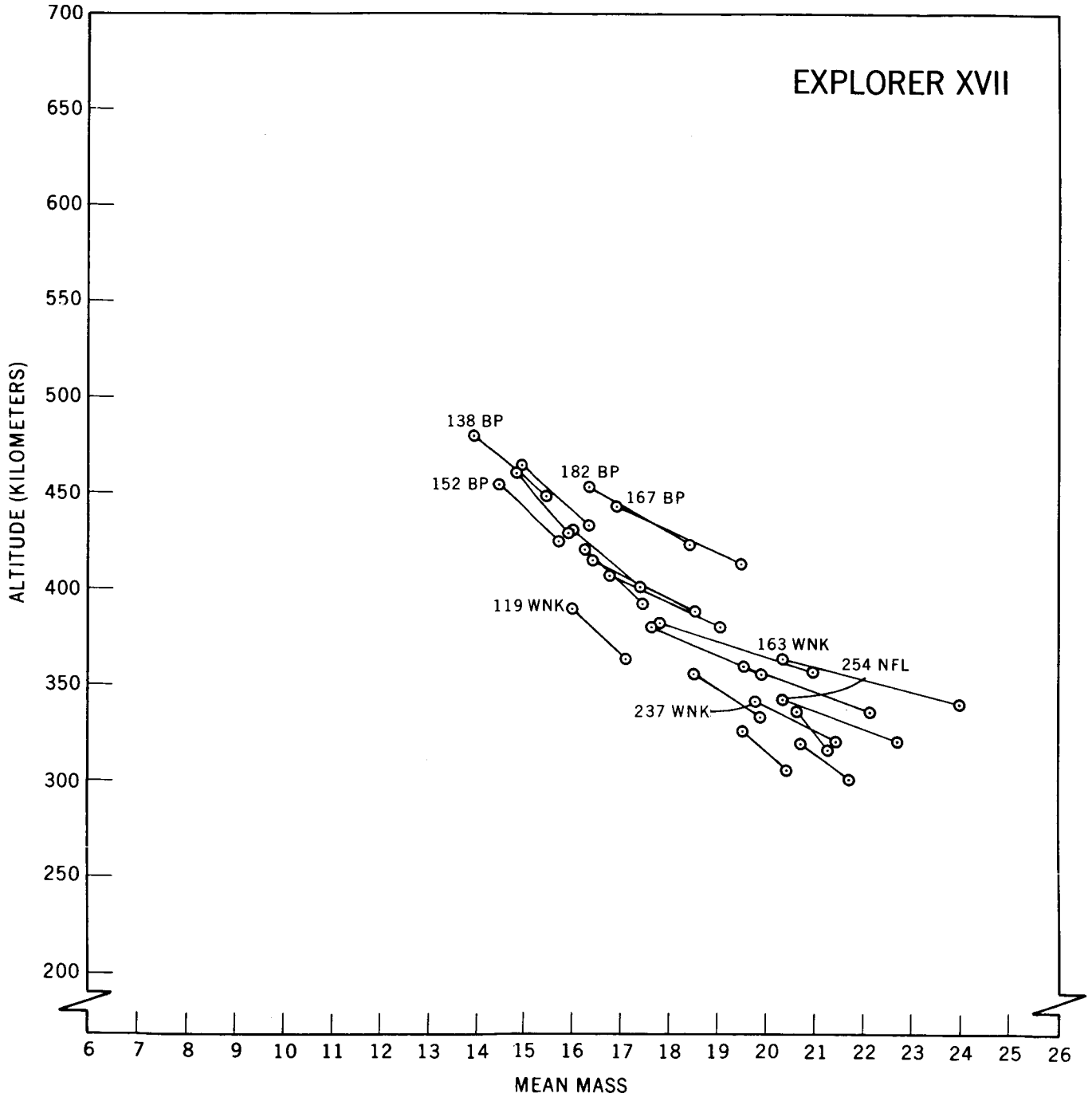
EXPLORER XVII
ALTITUDE (KILOMETERS)
700
650
600
550
500
450
400
350
300
250
200
6
7
8
9
10
11
12
13
14
15
16
17
18
19
20
21
22
23
24
25
26
MEAN MASS
138 BP
152 BP
182 BP
167 BP
119 WNK
163 WNK
254 NFL
237 WNK

FIGURE 9

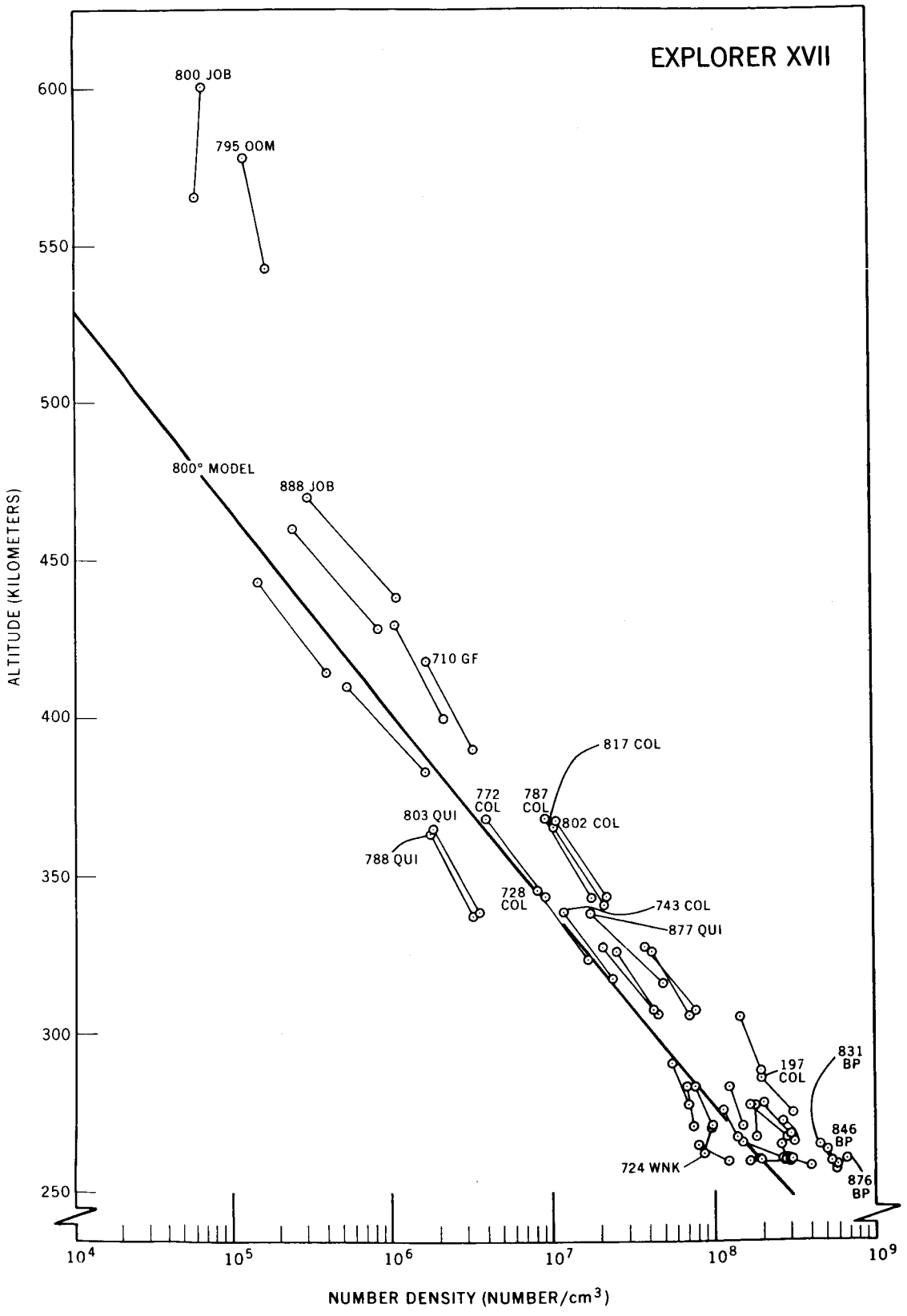
EXPLORER XVII
800 JOB
795 OOM
800° MODEL
888 JOB
710 GF
817 COL
772 COL
787 COL
803 QUI
802 COL
788 QUI
728 COL
743 COL
877 QUI
197 COL
831 BP
846 BP
724 WNK
876 BP
600
550
500
450
400
350
300
250
ALTITUDE (KILOMETERS)
10^4
10^5
10^6
10^7
10^8
10^9
NUMBER DENSITY (NUMBER/cm^3)

FIGURE 10

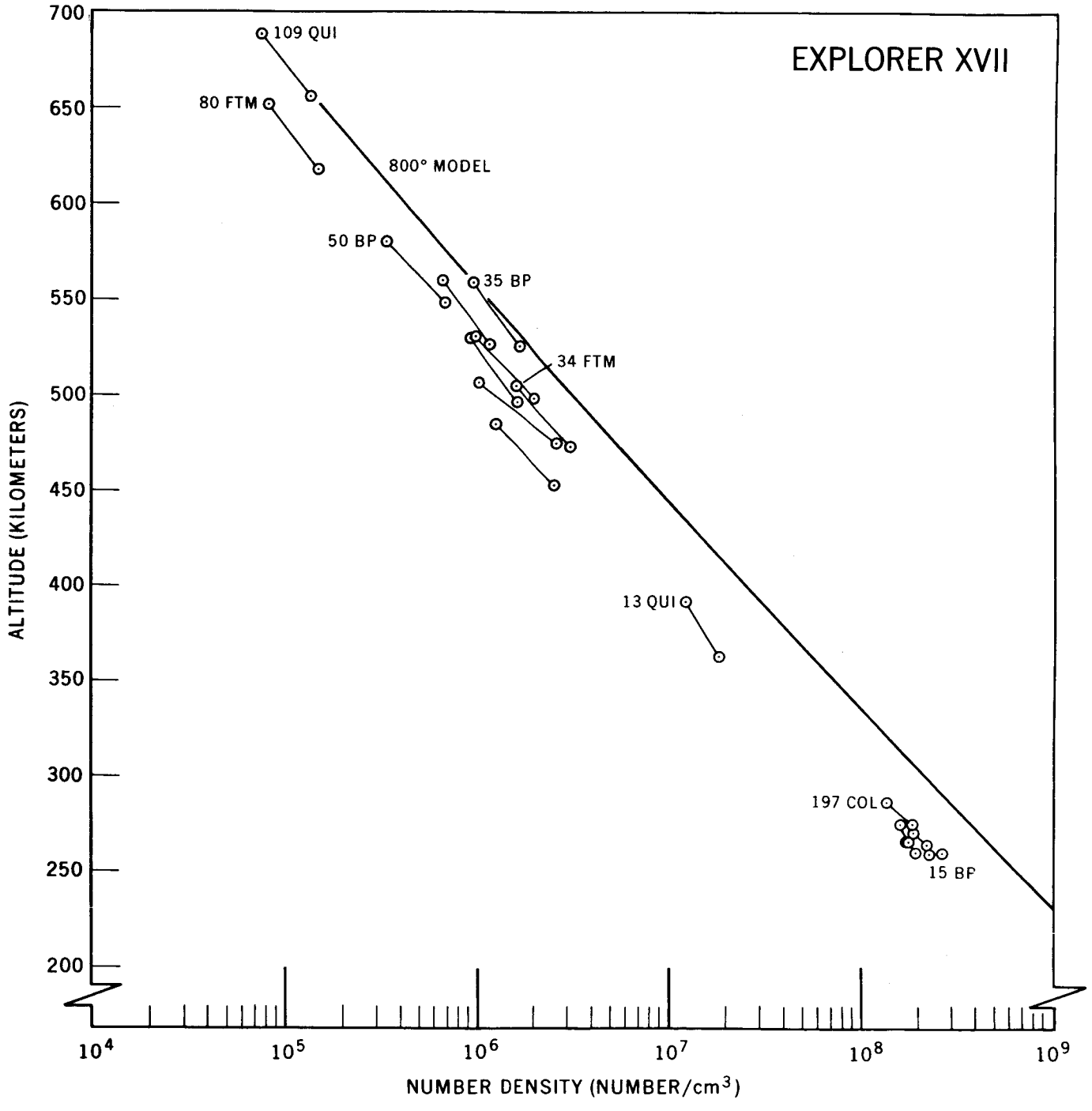
EXPLORER XVII
109 QUI
80 FTM
800° MODEL
50 BP
35 BP
34 FTM
13 QUI
197 COL
15 BP
ALTITUDE (KILOMETERS)
700
650
600
550
500
450
400
350
300
250
200
10^4
10^5
10^6
10^7
10^8
10^9
NUMBER DENSITY (NUMBER/cm^3)

FIGURE 11

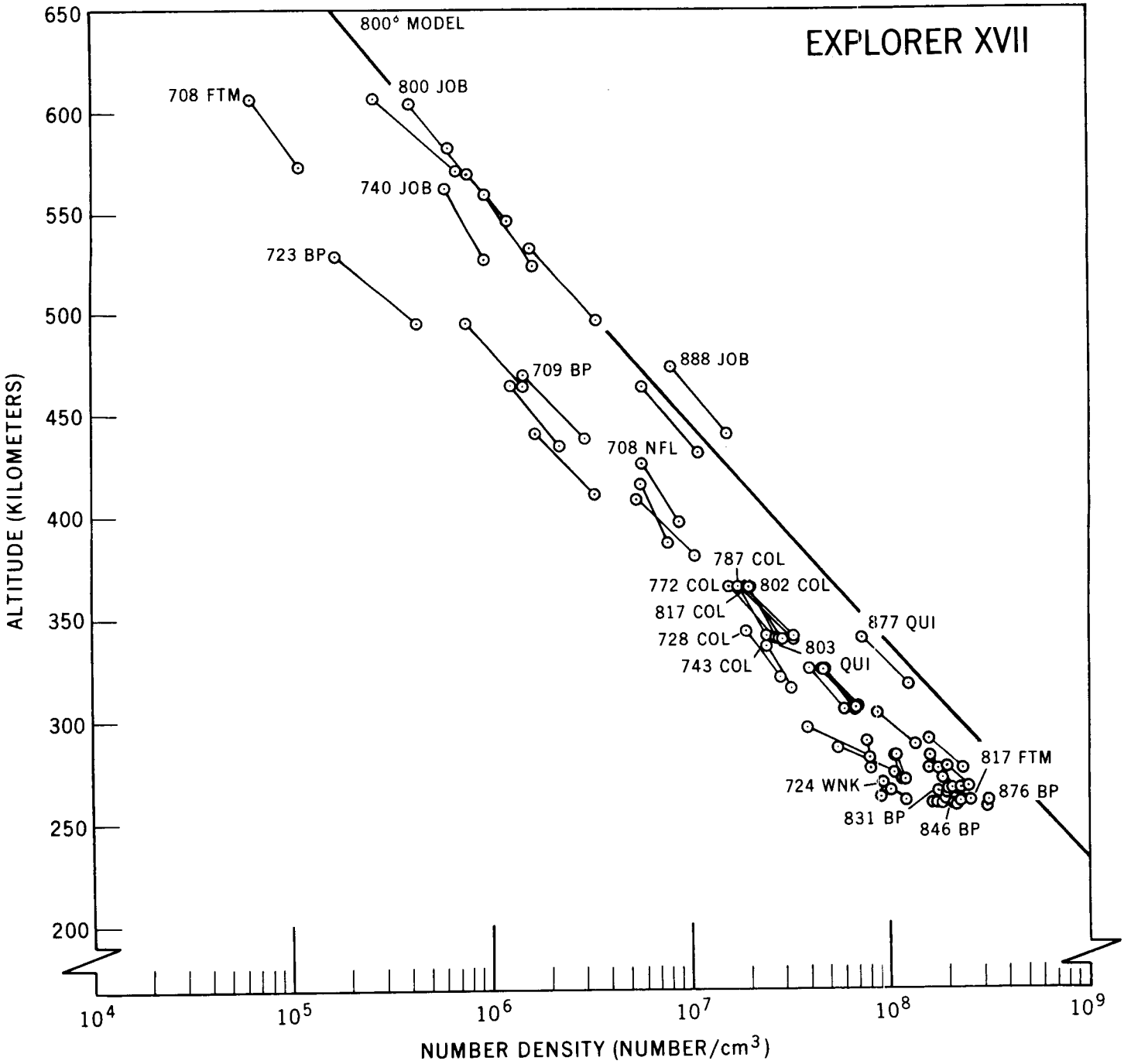
EXPLORER XVII
800° MODEL
800 JOB
708 FTM
740 JOB
723 BP
709 BP
888 JOB
708 NFL
787 COL
772 COL
802 COL
817 COL
728 COL
803
743 COL
QUI
877 QUI
817 FTM
724 WNK
876 BP
831 BP
846 BP
650
600
550
500
450
400
350
300
250
200
ALTITUDE (KILOMETERS)
10^4
10^5
10^6
10^7
10^8
10^9
NUMBER DENSITY (NUMBER/cm^3)

FIGURE 12

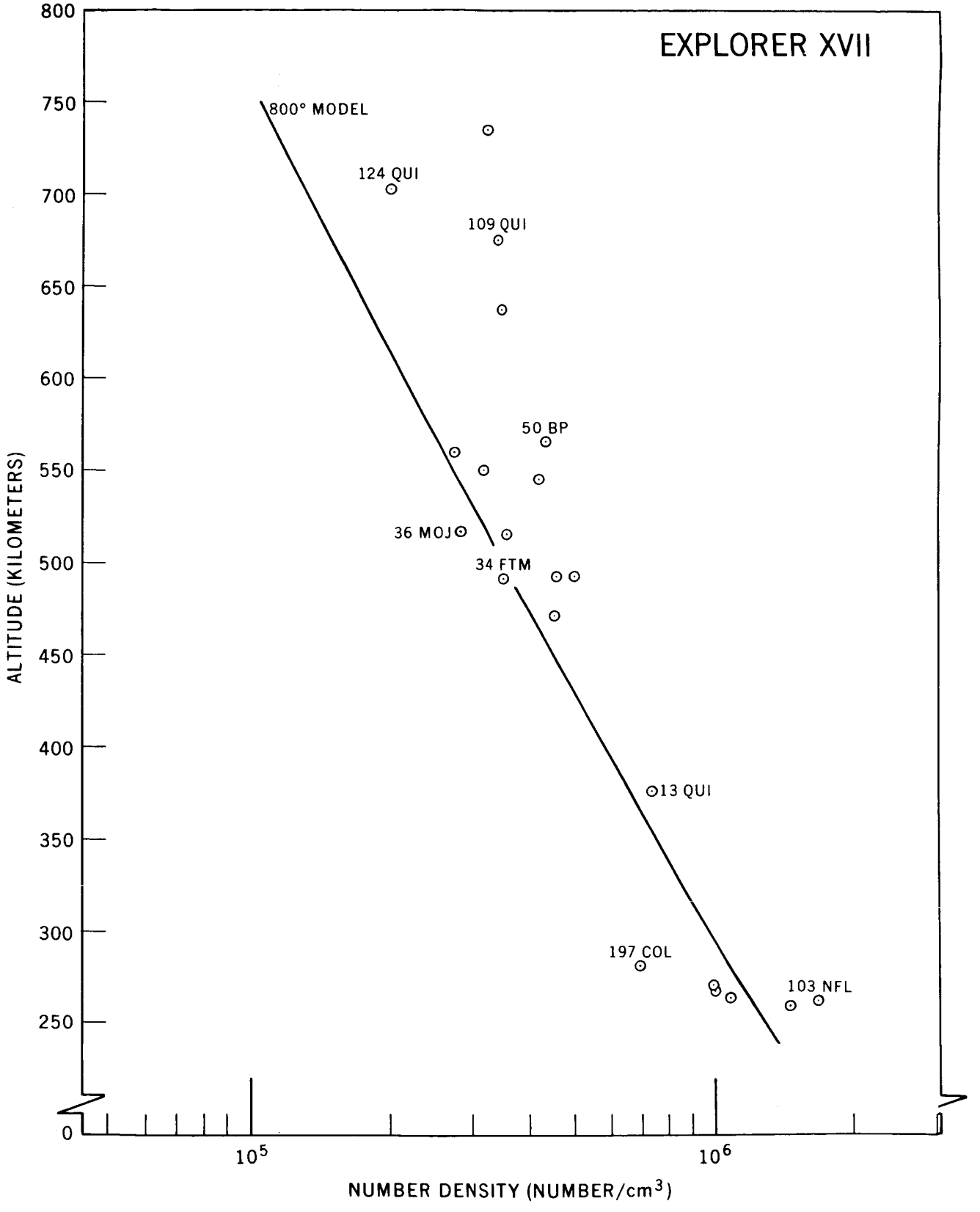
EXPLORER XVII
800° MODEL
124 QUI
109 QUI
50 BP
36 MOJ
34 FTM
13 QUI
197 COL
103 NFL
ALTITUDE (KILOMETERS)
800
750
700
650
600
550
500
450
400
350
300
250
0
10^5
10^6
NUMBER DENSITY (NUMBER/cm^3)

FIGURE 13

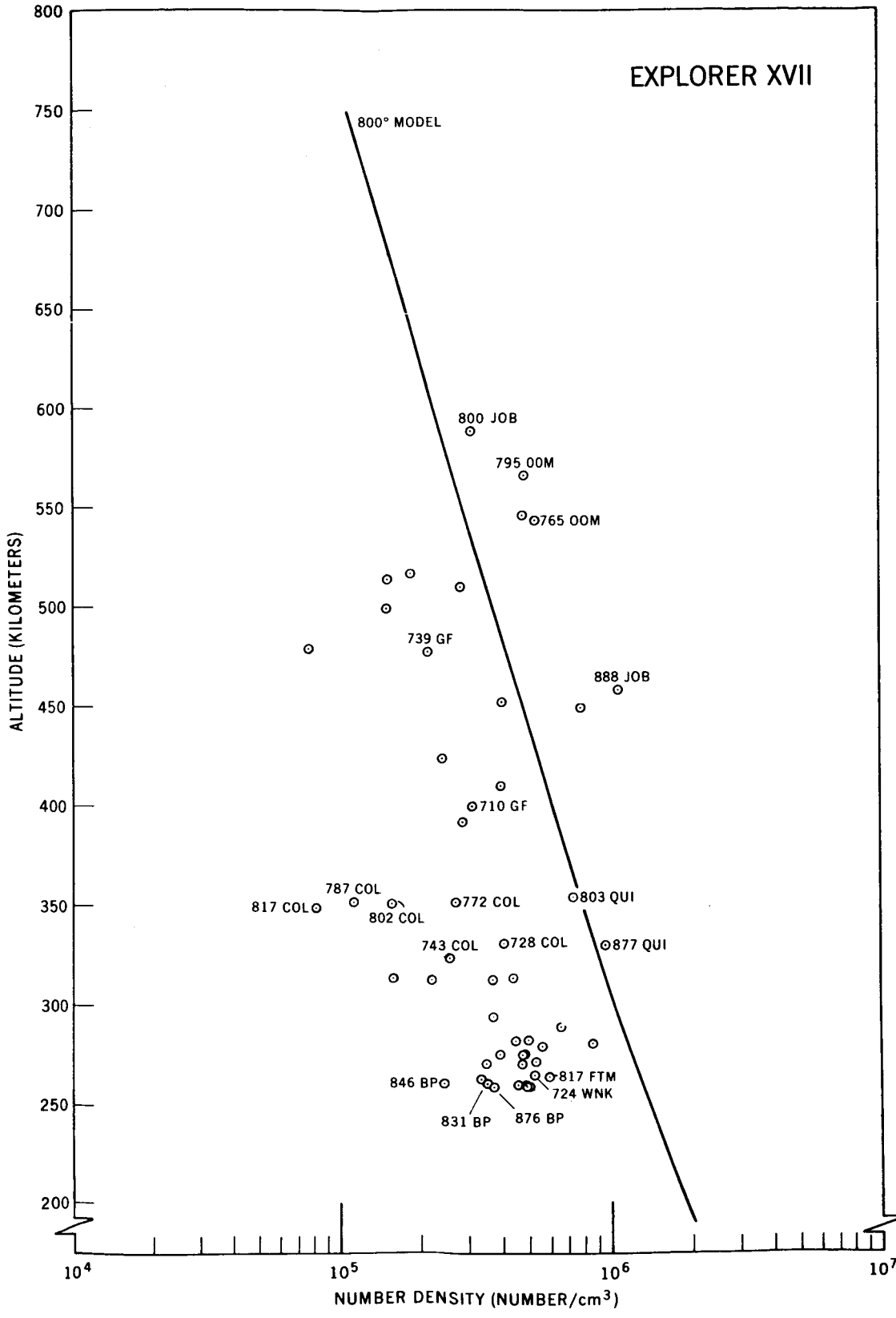
EXPLORER XVII
800° MODEL
800 JOB
795 OOM
765 OOM
739 GF
888 JOB
710 GF
787 COL
817 COL
802 COL
772 COL
803 QUI
743 COL
728 COL
877 QUI
846 BP
817 FTM
724 WNK
831 BP
876 BP
ALTITUDE (KILOMETERS)
NUMBER DENSITY (NUMBER/cm3)
800
750
700
650
600
550
500
450
400
350
300
250
200
10^4
10^5
10^6
10^7

FIGURE 14

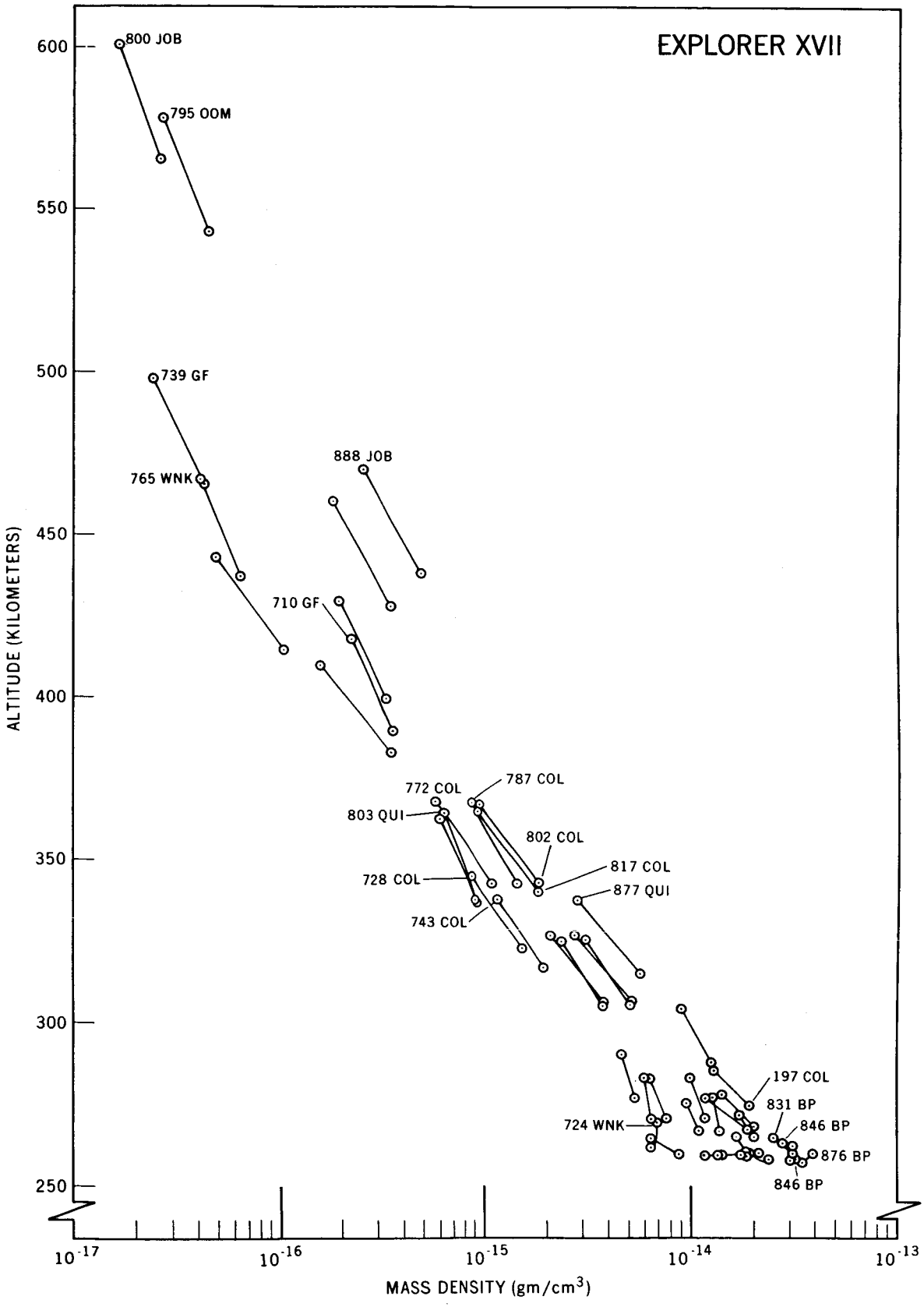
EXPLORER XVII
800 JOB
795 OOM
739 GF
765 WNK
888 JOB
710 GF
772 COL
787 COL
803 QUI
802 COL
817 COL
728 COL
877 QUI
743 COL
197 COL
831 BP
724 WNK
846 BP
876 BP
846 BP
600
550
500
450
400
350
300
250
ALTITUDE (KILOMETERS)
10^{-17}
10^{-16}
10^{-15}
10^{-14}
10^{-13}
MASS DENSITY (gm/cm^3)

FIGURE 15

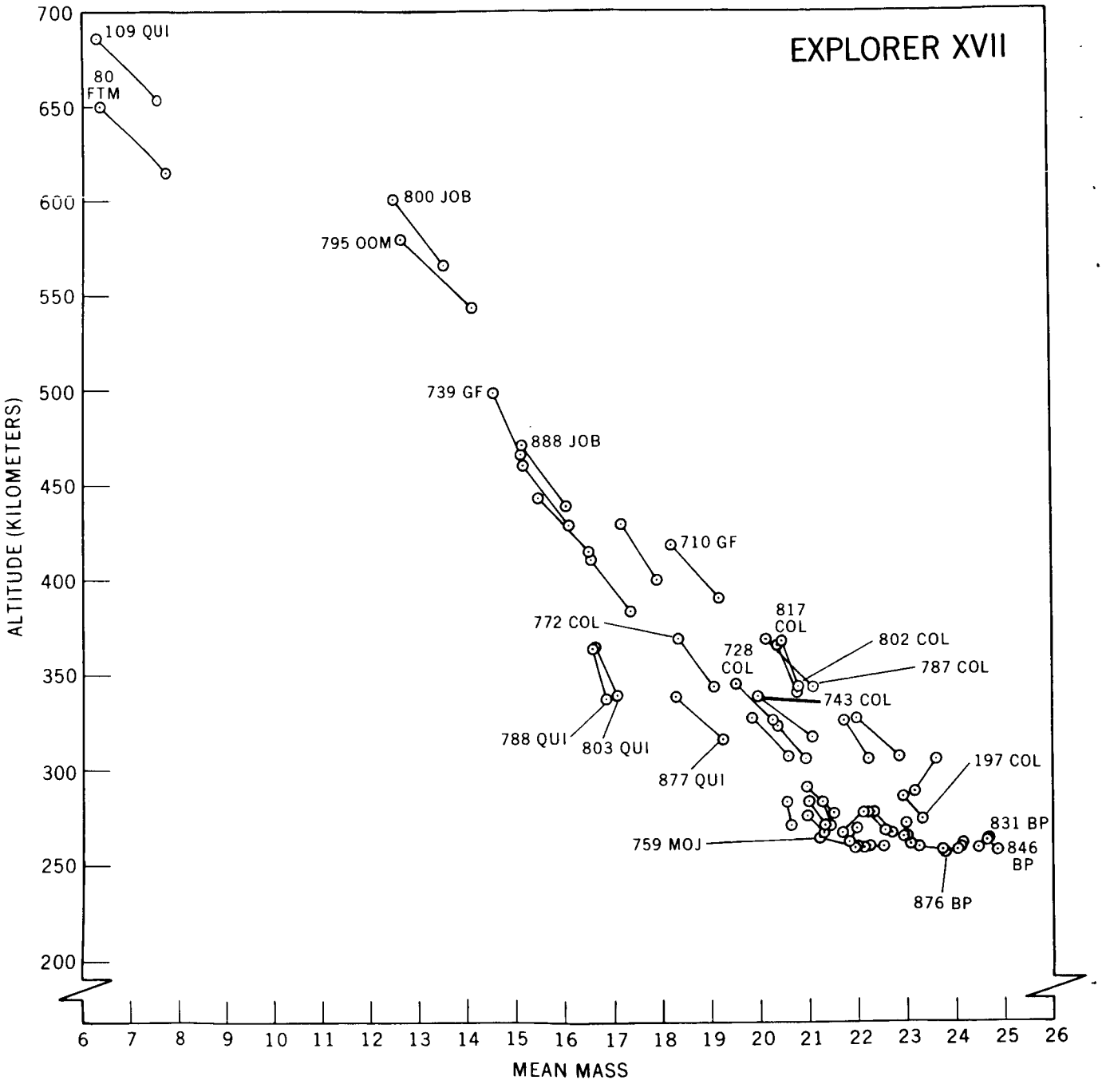
EXPLORER XVII
ALTITUDE (KILOMETERS)
MEAN MASS
700
650
600
550
500
450
400
350
300
250
200
6
7
8
9
10
11
12
13
14
15
16
17
18
19
20
21
22
23
24
25
26
109 QUI
80 FTM
800 JOB
795 OOM
739 GF
888 JOB
710 GF
772 COL
817 COL
802 COL
728 COL
787 COL
743 COL
788 QUI
803 QUI
877 QUI
197 COL
831 BP
759 MOJ
846 BP
876 BP

FIGURE 16

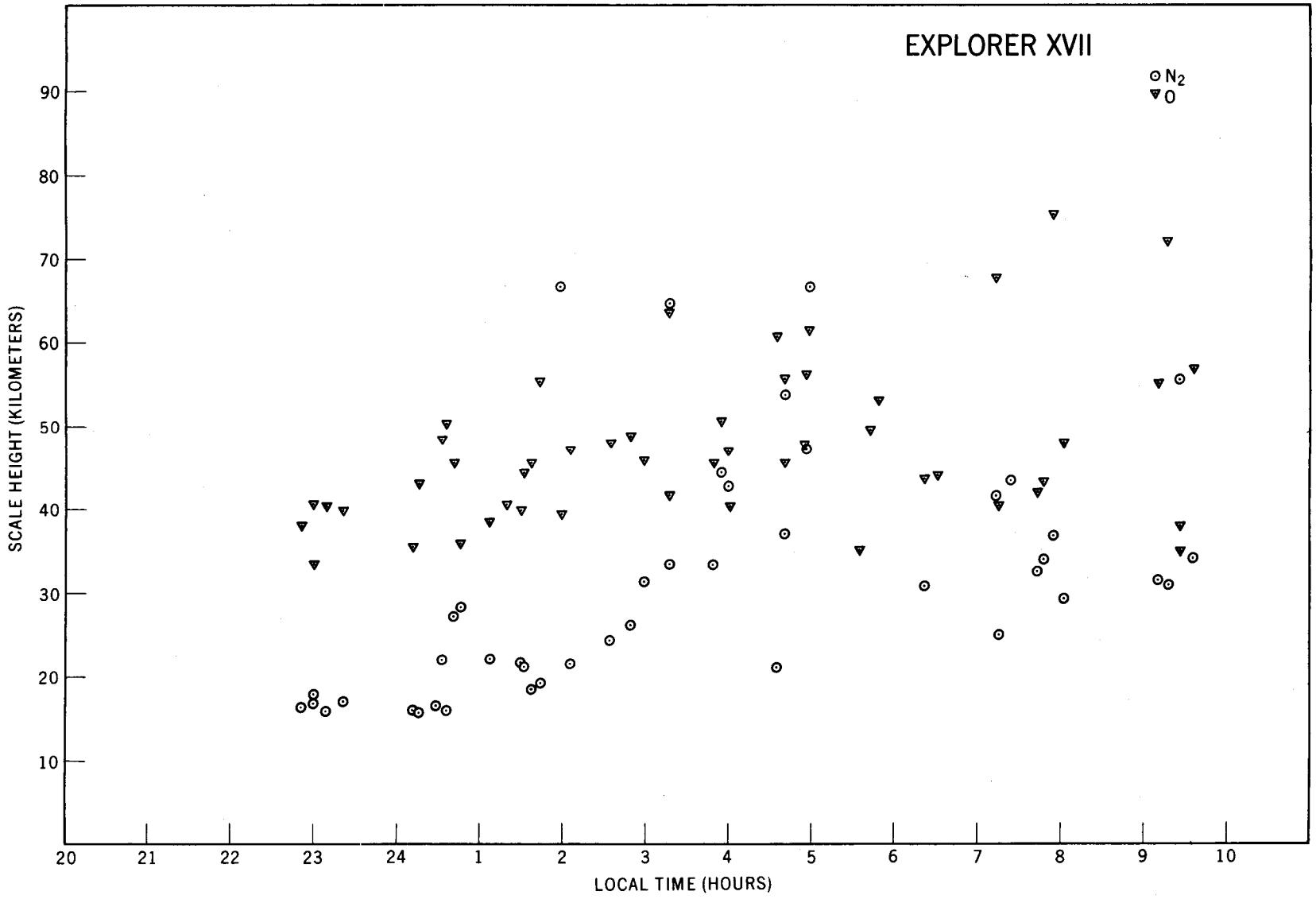
EXPLORER XVII
N_2
O
SCALE HEIGHT (KILOMETERS)
90
80
70
60
50
40
30
20
10
20
21
22
23
24
1
2
3
4
5
6
7
8
9
10
LOCAL TIME (HOURS)

FIGURE 17

TABLE 1

PASS	STATION	DATE	LOCAL TIME (hours)	ALTITUDE (kilometers)	GEOGRAPHIC LONGITUDE (degrees)	GEOGRAPHIC LATITUDE (degrees)	α (degrees)	A_p	$F_{10.7}$	NUMBER DENSITY He (number/cm^3)	NUMBER DENSITY N_2 (number/cm^3)	NUMBER DENSITY O (number/cm^3)
1	WNK	4/3/63	3.2	400	-10.1	54.6	56.8	4	74	6.91×10^5	9.27×10^6	8.36×10^6
			3.9	431	-0.6	51.5	63.3				6.65×10^6	5.97×10^6
4	NFL	4/3/63	4.5	472	-63.8	46.7	67.9	4	74	5.04×10^5		2.46×10^6
			5.0	506	-57.4	42.4	74.3				2.20×10^6	1.55×10^6
6	BPO	4/3/63	5.3	538	-101.0	38.0	78.7	4	74	2.79×10^5	4.49×10^6	1.21×10^6
			5.7	575	-96.2	33.1	85.1				2.87×10^6	8.01×10^5
7	MOJ	4/3/63	5.2	528	-126.8	39.2	77.4	4	74	3.20×10^5	4.18×10^6	1.29×10^6
			5.6	565	-121.8	34.3	83.9				3.00×10^6	9.07×10^5
13	QUI	4/4/63	18.9	395	-81.4	-5.3	60.3	19	70	7.39×10^5	3.95×10^6	1.23×10^7
			19.1	364	-78.1	0.7	53.4				4.44×10^6	1.84×10^7
15	BPO	4/4/63	20.9	260	-78.7	35.7	13.6	19	70	1.47×10^6	3.05×10^8	2.69×10^8
			21.3	259	-73.0	40.9	7.2				2.73×10^8	2.30×10^8
16	WNK	4/4/63	3.4	417	-8.8	52.2	51.3	19	70	6.21×10^5	2.78×10^6	4.88×10^6
			4.0	450	-0.3	48.6	57.9				1.36×10^6	2.55×10^6
18	NFL	4/4/63	3.5	420	-56.3	51.8	52.0	19	70	5.68×10^5	2.65×10^6	5.16×10^6
			4.1	453	-48.1	48.0	58.6				1.34×10^6	2.85×10^6
19	BPO	4/4/63	4.0	451	-73.0	48.2	57.4	19	70	4.58×10^5	1.77×10^6	2.59×10^6
			4.5	485	-65.9	43.9	64.1				8.90×10^5	1.27×10^6
20	BPO	4/4/63	4.9	524	-83.9	38.8	70.1	19	70		2.06×10^6	1.18×10^6
			5.3	560	-79.0	34.0	76.6				1.31×10^6	6.77×10^5
21	MOJ	4/4/63	4.6	495	-112.9	42.6	64.6	19	70	3.62×10^5	1.80×10^6	1.63×10^6
			5.0	530	-107.3	37.9	71.1				1.08×10^6	9.30×10^5
34	FTM	4/5/63	4.1	471	-73.4	44.7	54.6	32	72	3.55×10^5	1.64×10^6	3.11×10^6
			4.5	505	-67.3	40.2	61.1				6.52×10^5	1.61×10^6
35	BPO	4/5/63	4.7	523	-88.9	37.7	64.4	32	72	4.23×10^5	1.19×10^6	1.68×10^6
			5.1	559	-84.2	32.7	70.8				7.26×10^5	9.77×10^5
36	MOJ	4/5/63	4.4	495	-117.7	41.4	59.2	32	72	2.86×10^5	1.16×10^6	2.02×10^6
			4.8	531	-112.3	36.6	65.7				6.27×10^5	9.87×10^5
45	WNK	4/6/63	2.5	389	-1.3	53.7	33.8	19	78	3.86×10^5	7.67×10^6	9.66×10^6
			3.2	420	7.9	50.3	40.4				3.12×10^6	5.18×10^6
48	NFL	4/6/63	3.5	440	-60.0	47.6	42.7	19	78	6.13×10^5	1.86×10^6	5.66×10^6
			4.0	474	-53.1	43.2	49.3				7.34×10^5	2.85×10^6
49	BPO	4/6/63	3.9	472	-77.9	43.5	47.8	19	78	4.61×10^5	1.62×10^5	2.65×10^6
			4.3	507	-72.1	38.8	54.3					1.04×10^6
50	BPO	4/6/63	4.7	544	-91.2	33.5	61.0	19	78	4.39×10^5	2.35×10^5	6.93×10^5
			5.0	581	-86.9	28.4	67.5				2.06×10^5	3.41×10^5

TABLE 1—Continued

PASS	STATION	DATE	LOCAL TIME (hours)	ALTITUDE (kilometers)	GEOGRAPHIC LONGITUDE (degrees)	GEOGRAPHIC LATITUDE (degrees)	α (degrees)	A_p	$F_{10.7}$	NUMBER DENSITY He (number/cm^3)	NUMBER DENSITY N_2 (number/cm^3)	NUMBER DENSITY O (number/cm^3)
50	COL	4/6/63	0.1	316	-156.0	57.7	11.5	19	78	6.86×10^5	4.69×10^7	5.51×10^7
			1.0	338	-143.6	57.4	18.1				2.26×10^7	3.08×10^7
60	WNK	4/7/63	2.4	391	-4.7	52.7	27.3	15	80	5.94×10^5	4.57×10^6	1.09×10^7
			3.0	422	4.0	49.1	33.9				1.56×10^6	6.14×10^6
64	BPO	4/7/63	3.7	474	-82.3	42.0	42.4	15	80	3.42×10^5	6.73×10^5	2.37×10^6
			4.1	509	-76.7	37.3	48.9				3.16×10^5	1.19×10^6
65	QUI	4/7/63	5.7	715	-79.7	7.5	84.6	15	80	3.27×10^5	1.25×10^6	5.32×10^5
			5.9	748	-76.8	2.2	90.9				1.44×10^6	3.99×10^5
79	BPO	4/8/63	3.8	497	-83.5	37.7	39.3	7	81	5.97×10^5	1.69×10^5	1.47×10^6
			4.1	533	-78.6	32.7	45.8				1.20×10^5	6.44×10^5
79	COL	4/8/63	23.2	301	-148.2	57.4	8.7	7	81	8.65×10^5	7.91×10^7	7.96×10^7
			0.1	321	-135.7	57.6	4.3				3.02×10^7	3.95×10^7
80	FTM	4/8/63	4.7	615	-94.1	21.0	59.0	7	81	3.53×10^5	9.59×10^4	1.51×10^5
			5.0	652	-90.7	15.6	65.4				4.67×10^4	8.28×10^4
80	COL	4/8/63	0.5	333	-153.4	57.1	5.2	7	81	8.56×10^5	2.08×10^7	3.78×10^7
			1.3	358	-141.9	55.2	10.1				7.33×10^6	2.07×10^7
93	BPO	4/9/63	3.0	449	-72.0	43.2	24.2	7	82	6.81×10^5	2.86×10^5	2.30×10^6
			3.4	484	-66.2	38.4	30.7				1.12×10^5	1.40×10^6
103	NFL	4/9/63	20.0	261	-53.7	46.7	47.7	7	82	1.68×10^6	2.27×10^8	2.72×10^8
			20.6	263	-45.5	50.8	41.1					
109	QUI	4/10/63	4.5	653	-77.1	12.7	53.8	2	82	3.45×10^5	5.02×10^4	1.38×10^5
			4.7	689	-74.1	7.3	60.2				2.06×10^4	7.63×10^4
109	COL	4/10/63	23.2	306	-151.3	57.7	19.5	2	82	8.63×10^5	5.07×10^7	8.02×10^7
			0.1	327	-139.0	56.8	13.2				2.05×10^7	4.15×10^7
118	BPO	4/10/63	18.6	276	-75.5	34.2	73.5	2	82	1.00×10^6	1.14×10^8	1.61×10^8
			19.0	266	-69.9	39.6	66.7				1.38×10^8	1.73×10^8
119	WNK	4/11/63	1.1	363	-6.0	52.9	12.4	3	88	6.60×10^5	2.35×10^6	1.44×10^7
			1.7	391	2.9	49.3	8.8				6.85×10^5	8.00×10^6
120	GFO	4/11/63	19.9	261	-104.3	49.1	54.5	3	88	1.08×10^6	2.85×10^8	1.94×10^8
			20.6	266	-95.1	52.9	47.8				2.56×10^8	1.78×10^8
123	BPO	4/11/63	2.7	460	-79.7	39.4	13.2	3	88	7.47×10^5	1.74×10^5	1.85×10^6
			3.0	495	-74.6	34.4	18.6				8.53×10^4	1.02×10^6
124	QUI	4/11/63	4.4	681	-80.3	7.2	49.5	3	88	2.03×10^5	1.72×10^5	2.45×10^5
			4.6	716	-77.3	1.9	55.7				3.79×10^4	1.45×10^5
138	BPO	4/12/63	2.3	448	-86.7	40.0	10.0	9	93	4.82×10^5	3.08×10^5	3.07×10^6
			2.7	481	-81.5	35.1	12.2				8.61×10^4	1.60×10^6

TABLE 1—Continued

PASS	STATION	DATE	LOCAL TIME (hours)	ALTITUDE (kilometers)	GEOGRAPHIC LONGITUDE (degrees)	GEOGRAPHIC LATITUDE (degrees)	α (degrees)	A_p	$F_{10.7}$	NUMBER DENSITY He (number/cm^3)	NUMBER DENSITY N_2 (number/cm^3)	NUMBER DENSITY O (number/cm^3)
148	BPO	4/12/63	18.3	272	-83.2	38.9	84.9	9	93	1.01×10^6	2.62×10^8	1.90×10^8
			18.7	264	-76.8	43.9	78.2				3.08×10^8	2.23×10^8
151	NFL	4/13/63	0.9	373	-59.4	49.8	23.5	10	89	6.25×10^5	8.68×10^6	2.03×10^7
			1.5	402	-51.7	45.6	17.9					1.04×10^7
152	BPO	4/13/63	1.8	424	-71.4	42.3	15.2	10	89	5.00×10^5	3.88×10^5	4.52×10^6
			2.2	457	-65.7	37.5	11.6				9.57×10^4	2.38×10^6
163	WNK	4/14/63	24.0	340	-2.0	53.4	37.5	17	87	5.47×10^5	8.07×10^7	3.84×10^7
			0.6	365	7.2	50.0	31.3				1.94×10^7	3.11×10^7
167	BPO	4/14/63	1.4	413	-78.2	42.7	23.1	17	87	4.49×10^5	4.56×10^6	8.74×10^6
			1.8	446	-72.3	37.8	17.8				9.71×10^5	5.10×10^6
182	BPO	4/15/63	1.3	423	-81.1	40.1	27.7	15	88	4.33×10^5	3.30×10^6	1.00×10^7
			1.7	456	-75.8	35.1	22.2				6.47×10^5	5.17×10^6
183	QUI	4/15/63	3.1	641	-81.0	7.7	19.4	15	88	3.09×10^5	7.60×10^4	1.83×10^5
			3.3	678	-78.0	2.3	24.5				4.54×10^4	8.24×10^4
197	COL	4/16/63	20.7	274	-149.4	57.6	74.6	6	88	6.94×10^5	3.03×10^8	1.87×10^8
			21.5	287	-136.9	57.6	68.1				1.97×10^8	1.38×10^8
197	BPO	4/16/63	1.2	433	-84.1	37.3	30.4	6	88	4.43×10^5	6.43×10^5	5.22×10^6
			1.6	467	-79.3	32.2	24.6				1.56×10^5	2.43×10^6
211	BPO	4/17/63	0.3	380	-74.9	44.5	49.0	7	87	4.04×10^5	6.12×10^6	1.51×10^7
			0.7	409	-68.8	39.9	42.8				1.12×10^6	8.79×10^6
219	OOM	4/17/63	3.6	802	136.2	-20.3	28.2	7	87	1.64×10^5	1.47×10^5	1.26×10^5
			3.8	830	139.5	-25.2	33.6				8.46×10^4	5.86×10^4
226	BPO	4/18/63	0.3	392	-76.9	41.5	57.1	15	88	4.22×10^5	2.13×10^6	1.09×10^7
			0.7	422	-71.4	36.6	50.9				5.97×10^5	6.10×10^6
237	WNK	4/18/63	22.6	321	-6.2	52.3	80.3	15	88	7.69×10^5	8.48×10^7	9.56×10^7
			23.2	343	3.1	48.8	73.9				2.77×10^7	5.24×10^7
241	BPO	4/19/63	24.0	388	-82.5	41.0	65.1	10	84	4.99×10^5	5.09×10^6	1.54×10^7
			0.4	418	-77.0	36.1	58.9				8.60×10^5	8.03×10^6
242	QUI	4/19/63	1.8	601	-81.7	8.4	29.5	10	84	3.26×10^5	1.30×10^4	1.96×10^5
			2.0	638	-78.6	3.0	24.8				7.76×10^3	8.27×10^4
243	MOJ	4/19/63	0.5	429	-124.0	34.2	57.6	10	84	4.46×10^5	4.08×10^5	4.66×10^6
			0.8	462	-119.5	28.9	51.5				1.33×10^5	2.37×10^6
249	OOM	4/19/63	3.1	812	126.7	-24.4	22.2	10	84	2.25×10^5	8.65×10^4	8.00×10^4
			3.4	839	130.2	-29.2	26.2				2.90×10^4	
254	NFL	4/20/63	22.4	321	-57.7	51.4	85.6	7	78	6.29×10^5	8.13×10^7	6.00×10^7
			23.0	344	-49.3	47.5	79.2				2.24×10^7	3.43×10^7

TABLE 1—Continued

PASS	STATION	DATE	LOCAL TIME (hours)	ALTITUDE (kilometers)	GEOGRAPHIC LONGITUDE (degrees)	GEOGRAPHIC LATITUDE (degrees)	α (degrees)	A_p	$F_{10.7}$	NUMBER DENSITY He (number/cm^3)	NUMBER DENSITY N_2 (number/cm^3)	NUMBER DENSITY O (number/cm^3)
256	BPO	4/20/63	23.9	401	-84.7	37.5	66.5	7	78	2.58×10^5	1.64×10^6	9.32×10^6
			0.3	433	-79.7	32.4	60.3				2.64×10^5	4.11×10^6
270	BPO	4/21/63	23.0	355	-74.8	44.3	83.5	4	74	5.97×10^5	1.19×10^7	2.13×10^7
			23.5	382	-68.6	39.6	77.1				2.73×10^6	1.13×10^7
271	GFO	4/21/63	22.6	336	-104.7	47.7	88.4	4	74	4.10×10^5	3.35×10^7	2.95×10^7
			23.1	361	-97.6	43.2	81.9				8.30×10^6	1.65×10^7
285	BPO	4/22/63	22.8	357	-78.9	42.9	90.3	11	72	8.97×10^5	1.50×10^7	1.73×10^7
			23.3	385	-73.0	38.0	83.8				3.01×10^6	9.15×10^6
287	QUI	4/22/63	1.4	658	-93.2	-4.0	36.1	11	72	4.71×10^5		
			1.6	694	-90.2	-9.3	30.3					
708	FTM	5/20/63	4.9	610	-80.8	21.5	76.4	8	91	3.19×10^5		6.47×10^4
			5.2	573	-77.0	26.9	69.8					1.13×10^5
708	NFL	5/20/63	6.8	429	-54.6	47.2	42.7	8	91	3.99×10^5	1.06×10^6	5.82×10^6
			7.4	397	-46.4	51.1	36.0				2.14×10^6	8.92×10^6
709	BPO	5/20/63	6.2	472	-87.5	41.4	51.5	8	91	4.00×10^5		1.48×10^6
			6.7	438	-80.9	46.0	44.8				3.16×10^5	3.02×10^6
710	GFO	5/20/63	7.0	418	-100.6	48.6	40.9	8	91	3.12×10^5	1.68×10^6	5.77×10^6
			7.6	387	-91.8	52.4	34.2				3.26×10^6	7.86×10^6
723	BPO	5/21/63	5.3	531	-76.7	34.1	68.7	5	88	2.82×10^5		1.72×10^5
			5.7	495	-71.5	39.1	62.0				4.73×10^3	4.34×10^5
724	WNK	5/21/63	12.1	269	-3.4	51.6	4.3	5	88	5.29×10^5	9.48×10^7	9.32×10^7
			12.7	262	5.4	47.4	7.7				8.67×10^7	9.06×10^7
728	COL	5/21/63	8.6	345	-151.1	56.9	32.1	5	88	4.12×10^5	8.20×10^6	1.91×10^7
			9.4	321	-138.4	57.8	25.3				1.66×10^7	2.84×10^7
736	WNK	5/22/63	6.8	410	-8.9	51.2	50.1	3	89	2.88×10^5	5.39×10^5	5.48×10^6
			7.5	380	0.7	54.4	43.4				1.62×10^6	1.08×10^7
738	WNK	5/22/63	10.7	291	-0.6	56.0	19.5	3	89	4.52×10^5	5.53×10^7	7.71×10^7
			11.5	276	10.5	53.2	13.0				6.92×10^7	8.06×10^7
738	BPO	5/22/63	5.0	535	-81.7	34.7	76.2	3	89	1.51×10^5	2.73×10^5	3.57×10^5
			5.4	500	-76.5	39.7	69.7				5.81×10^4	5.25×10^5
739	GFO	5/22/63	5.4	498	-100.6	40.0	70.3	3	89	2.14×10^5	8.85×10^4	7.78×10^5
			5.9	464	-94.4	44.6	63.6				8.41×10^4	1.48×10^6
740	JOB	5/22/63	16.3	523	29.5	-24.1	83.1	3	89	4.74×10^5	4.72×10^4	9.61×10^5
			16.7	562	33.6	-29.6	89.8				1.53×10^5	6.18×10^5
743	COL	5/22/63	8.7	338	-150.4	57.5	37.3	3	89	2.59×10^5	1.19×10^7	2.41×10^7
			9.5	315	-137.6	57.7	30.6				2.37×10^7	3.23×10^7

TABLE 1—Continued

PASS	STATION	DATE	LOCAL TIME (hours)	ALTITUDE (kilometers)	GEOGRAPHIC LONGITUDE (degrees)	GEOGRAPHIC LATITUDE (degrees)	α (degrees)	A_p	$F_{10.7}$	NUMBER DENSITY He (number/cm^3)	NUMBER DENSITY N_2 (number/cm^3)	NUMBER DENSITY O (number/cm^3)
753	WNK	5/23/63	10.9	283	1.8	54.2	23.1	3	93	4.89×10^5	7.65×10^7	1.07×10^8
			11.6	270	11.8	50.7	16.7				9.65×10^7	1.20×10^8
753	BPO	5/23/63	4.8	538	-86.5	35.6	83.3	3	93	1.84×10^5	2.23×10^5	3.94×10^5
			5.1	503	-81.3	40.4	76.7				1.01×10^5	5.12×10^5
754	GFO	5/23/63	6.0	443	-93.9	48.3	66.4	3	93	2.42×10^5	1.48×10^5	1.70×10^6
			6.6	411	-85.4	52.1	59.8				3.91×10^5	3.35×10^6
758	COL	5/23/63	9.0	326	-146.7	57.8	40.5	3	93	3.73×10^5	2.53×10^7	4.65×10^7
			9.8	305	-134.1	56.9	33.9				4.51×10^7	6.54×10^7
758	FTM	5/23/63	13.8	280	-77.8	23.2	20.2	3	93	6.63×10^5		7.96×10^7
			14.1	296	-73.8	17.2	26.8					3.90×10^7
759	MOJ	5/23/63	13.0	259	-113.4	36.7	8.6	3	93	3.34×10^5	1.21×10^8	1.20×10^8
			13.4	265	-108.1	31.0	11.9				7.98×10^7	1.01×10^8
765	WNK	5/24/63	5.4	467	-6.0	46.0	75.3	2	89		2.17×10^5	1.29×10^6
			6.0	434	1.7	50.1	68.8				1.38×10^5	2.29×10^6
765	OOM	5/24/63	15.9	520	141.3	-25.8	72.4	2	89	5.32×10^5		1.68×10^6
			16.2	559	145.5	-31.1	78.9				1.33×10^5	9.56×10^5
768	WNK	5/24/63	10.7	283	-1.8	53.6	30.1	2	89	4.80×10^5	6.72×10^7	1.09×10^8
			11.4	271	7.9	49.9	23.7				7.41×10^7	1.16×10^8
768	BPO	5/24/63	4.7	519	-88.1	39.4	86.3	2	89	1.50×10^5	3.36×10^5	6.43×10^5
			5.2	484	-82.2	44.0	79.8				6.92×10^4	6.99×10^5
772	BPO	5/24/63	12.2	259	-76.4	42.0	15.9	2	89	5.07×10^5	1.95×10^8	1.83×10^8
			12.7	259	-70.3	36.7	11.6				1.66×10^8	1.64×10^8
772	COL	5/24/63	7.4	368	-145.6	56.6	57.6	2	89	2.73×10^5	3.94×10^6	1.59×10^7
			8.3	341	-133.3	57.7	51.0				9.10×10^6	2.64×10^7
773	FTM	5/24/63	13.4	272	-85.0	25.4	13.0	2	89	5.64×10^5	7.08×10^7	1.06×10^8
			13.7	286	-80.8	19.4	18.1				1.64×10^7	5.49×10^7
773	COL	5/24/63	8.8	327	-149.9	57.7	47.6	2	89	4.43×10^5	2.07×10^7	4.51×10^7
			9.7	306	-137.5	56.6	41.1				4.29×10^7	6.99×10^7
783	WNK	5/25/63	10.5	283	-5.2	52.9	38.8	8	83	3.92×10^5	1.25×10^8	1.60×10^8
			11.2	271	4.1	49.1	32.3				1.50×10^8	1.83×10^8
783	BPO	5/25/63	4.7	499	-89.0	43.2	90.3	8	83	7.75×10^4	6.85×10^5	1.19×10^6
			5.2	465	-82.2	47.5	83.9				2.35×10^5	1.15×10^6
785	NFL	5/25/63	10.8	277	-49.1	51.1	36.2	8	83	4.77×10^5	1.79×10^8	1.74×10^8
			11.4	266	-40.6	46.9	29.9				1.83×10^8	2.04×10^8
787	BPO	5/25/63	12.1	259	-78.9	39.5	22.8	8	83	4.92×10^5	2.58×10^8	2.15×10^8
			12.5	259	-73.3	34.1	17.4				1.87×10^8	1.75×10^8

TABLE 1—Continued

PASS	STATION	DATE	LOCAL TIME (hours)	ALTITUDE (kilometers)	GEOGRAPHIC LONGITUDE (degrees)	GEOGRAPHIC LATITUDE (degrees)	α (degrees)	A_p	$F_{10.7}$	NUMBER DENSITY He (number/cm^3)	NUMBER DENSITY N_2 (number/cm^3)	NUMBER DENSITY O (number/cm^3)
787	COL	5/25/63	7.3	368	-148.4	57.0	66.3	8	83	1.14×10^5	9.04×10^6	1.75×10^7
			8.2	341	-135.9	57.8	59.7				1.76×10^7	2.42×10^7
788	COL	5/25/63	8.7	327	-152.6	57.6	56.7	8	83	1.59×10^5	3.76×10^7	3.94×10^7
			9.5	305	-140.3	56.2	50.1				7.77×10^7	5.99×10^7
788	QUI	5/25/63	14.0	337	-77.0	3.6	25.2	8	83		3.21×10^6	2.91×10^7
			14.3	366	-73.6	-2.6	31.4				1.77×10^6	1.92×10^7
789	SNT	5/25/63	15.9	568	-76.8	-34.1	66.8	8	83	1.41×10^4	7.84×10^4	6.99×10^5
			16.2	607	-71.8	-39.0	73.2					2.70×10^5
795	OOM	5/26/63	15.5	543	134.5	-31.4	59.4	6	76	4.83×10^5	1.66×10^5	1.25×10^6
			15.9	582	139.1	-36.3	65.7				1.20×10^5	6.33×10^5
800	NFL	5/26/63	10.6	278	-53.6	50.6	45.3	6	76	5.34×10^5	2.01×10^8	1.91×10^8
			11.2	267	-45.3	46.4	38.8				2.95×10^8	2.48×10^8
800	JOB	5/26/63	15.7	566	15.6	-34.7	61.0	6	76	3.07×10^5	5.95×10^4	7.81×10^5
			16.0	604	20.7	-39.5	67.3				6.62×10^4	4.07×10^5
802	COL	5/26/63	7.2	367	-150.9	57.3	73.9	6	76	1.57×10^5	1.06×10^7	1.90×10^7
			8.0	341	-138.4	57.8	67.3				2.16×10^7	3.32×10^7
802	BPO	5/26/63	12.0	258	-81.4	36.7	27.5	6	76	4.86×10^5	3.92×10^8	2.17×10^8
			12.4	260	-76.3	31.2	21.6				2.96×10^8	1.88×10^8
803	QUI	5/26/63	13.8	338	-81.8	2.1	18.8	6	76	7.38×10^5	3.53×10^6	2.73×10^7
			14.0	366	-78.4	-3.9	24.5				1.81×10^6	1.96×10^7
803	COL	5/26/63	8.6	326	-154.8	57.3	63.7	6	76	2.21×10^5	4.13×10^7	4.68×10^7
			9.4	305	-142.8	55.6	57.1				7.09×10^7	6.92×10^7
815	NFL	5/27/63	10.4	277	-56.6	49.5	51.7	7	80	3.49×10^5	1.69×10^8	1.58×10^8
			11.0	266	-48.8	45.1	45.1				2.81×10^8	2.28×10^8
817	COL	5/27/63	7.1	365	-152.8	57.6	80.7	7	80	8.28×10^4	1.01×10^7	1.88×10^7
			8.0	339	-140.3	57.6	74.1				2.12×10^7	3.32×10^7
817	FTM	5/27/63	12.1	260	-81.2	30.3	28.3	7	80	5.96×10^5	2.76×10^8	2.54×10^8
			12.4	266	-76.7	24.6	22.1				1.50×10^8	1.95×10^8
831	BPO	5/28/63	10.8	264	-76.2	43.3	52.6	16	79	3.53×10^5	4.51×10^8	1.76×10^8
			11.3	259	-70.0	38.3	46.0				5.43×10^8	2.28×10^8
833	SNT	5/28/63	14.5	494	-74.5	-27.8	32.9	16	79	1.53×10^5	6.79×10^4	3.44×10^6
			14.8	532	-70.2	-32.9	39.1				2.96×10^4	1.61×10^6
842	WNK	5/29/63	8.9	305	-7.5	54.2	77.9	21	80	3.72×10^5	1.45×10^8	8.76×10^7
			9.6	287	2.3	50.9	71.2				1.95×10^8	1.35×10^8
846	BPO	5/29/63	10.7	263	-79.3	41.5	59.3	21	80	2.45×10^5	4.92×10^8	1.91×10^8
			11.1	258	-73.4	36.4	52.6				5.77×10^8	2.04×10^8

TABLE 1—Continued

PASS	STATION	DATE	LOCAL TIME (hours)	ALTITUDE (kilometers)	GEOGRAPHIC LONGITUDE (degrees)	GEOGRAPHIC LATITUDE (degrees)	α (degrees)	A_p	$F_{10.7}$	NUMBER DENSITY He (number/cm^3)	NUMBER DENSITY N_2 (number/cm^3)	NUMBER DENSITY 0 (number/cm^3)
861	BPO	5/30/63	10.5	262	-82.4	39.5	70.1	12	83	4.56×10^5	5.29×10^8	2.50×10^8
			10.9	257	-76.9	34.2	63.7				5.20×10^8	2.52×10^8
873	JOB	5/31/63	13.3	428	26.0	-21.1	22.5	9	89	7.83×10^5	8.35×10^5	1.11×10^7
			13.5	463	29.8	-26.5	21.9				2.42×10^5	5.83×10^6
874	NFL	5/31/63	9.0	291	-55.6	50.0	92.3	9	89	5.00×10^5	4.19×10^8	1.58×10^8
			9.6	276	-47.6	45.8	86.0				4.77×10^8	2.32×10^8
876	BPO	5/31/63	10.3	260	-85.4	37.2	77.0	9	89	3.73×10^5	6.62×10^8	3.15×10^8
			10.7	257	-80.2	31.8	70.9				5.72×10^8	3.09×10^8
877	QUI	5/31/63	12.2	316	-84.5	0.9	41.8	9	89	9.74×10^5	4.84×10^7	1.24×10^8
			12.4	340	-81.2	-5.0	36.7				1.73×10^7	7.30×10^7
888	JOB	6/1/63	13.1	438	22.3	-23.8	33.2	11	84	1.09×10^6	1.09×10^6	1.55×10^7
			13.4	473	26.3	-29.1	31.6				3.06×10^5	8.20×10^6